PREPARATION OF BARIUM DOPED BAGHDADITE/PHBV FIBROUS SCAFFOLDS FOR BONE TISSUE ENGINEERING

A THESIS SUBMITTED TO
THE GRADUATE SCHOOL OF NATURAL AND APPLIED SCIENCES
OF
MIDDLE EAST TECHNICAL UNIVERSITY

BY

SANAOSSADAT SADREDDINI

IN PARTIAL FULFILLMENT OF THE REQUIREMENTS
FOR
THE DEGREE OF MASTER OF SCIENCE
IN
BIOMEDICAL ENGINEERING

JANUARY 2023

Approval of the thesis:

PREPARATION OF BARIUM DOPED BAGHDADITE/PHBV FIBROUS SCAFFOLDS FOR BONE TISSUE ENGINEERING

Submitted by **Sanaossadat Sadreddini** in partial fulfillment of the requirements for the degree of i**n Biomedical Engineering, Middle East Technical University** by,

Prof. Dr. Halil Kalıpçılar
Dean, Graduate School of **Natural and Applied Sciences** _____

Prof. Dr. Vilda Purutcuoglu
Head of the Department, **Biomedical Engineering** _____

Prof. Dr. Zafer Evis
Supervisor, **Engineering Sciences, METU** _____

Prof. Dr. Dilek Keskin
Co-Supervisor, **Engineering Sciences, METU** _____

Examining Committee Members:

Prof. Dr. Ayşen Tezcaner
Engineering Sciences, METU _____

Prof. Dr. Zafer Evis
Engineering Sciences, METU _____

Prof. Dr. Dilek Keskin
Engineering Sciences, METU _____

Prof. Dr. Fatih Akkurt
Chemical Engineering, Gazi University _____

Assist. Prof. Dr. Yasin Sarikavak
Mechanical Engineering, Ankara Yıldırım Beyazıt University _____

Date: 23.01.2023

I hereby declare that all information in this document has been obtained and presented in accordance with academic rules and ethical conduct. I also declare that, as required by these rules and conduct, I have fully cited and referenced all material and results that are not original to this work.

Name Last name: Sanaossadat Sadreddini

Signature:

ABSTRACT

PREPERATION OF BARIUM DOPED BAGHDADITE/PHBV FIBROUS SCAFFOLDS FOR BONE TISSUE ENGINEERING

Sadreddini, Sanaossadat
Master of Science, Biomedical Engineering
Supervisor: Prof. Dr. Zafer Evis
Co-Supervisor: Prof. Dr. Dilek Keskin

January 2023, 78 pages

Recently, bioceramic/polymer composites have dragged a lot of attention for treating hard tissue damages using bone tissue engineering (BTE). In this context, it was aimed to develop fibrous composite poly(hydroxybutyrate) co (hydroxyvalerate)-polycaprolactone, PHBV-PCL, scaffolds containing different amounts of baghdadite (BAG) and Ba-doped BAG that can provide bone regeneration in the bone defect area and to investigate the effect of these scaffolds on the structural, mechanical, and biological properties. BAG and Ba-doped BAGs were synthesized using the sol-gel method and sintered at 1150^{o}C. Microstructural and biological characterization results were evaluated and 4 different groups were selected for scaffold constructions. PHBV/PCL composite scaffolds containing different amounts of BAG and Ba-doped BAG (1, 3, and 5 wt%) were produced by the wet electrospinning method with a porosity of 72-78%. The presence of Ba-doped BAG in the PHBV scaffolds resulted in increasing bioactivity, cell viability, and ALP activity, and it was introduced as a suitable way to control the degradation rate of scaffolds. The presence of BAG in the scaffolds improved the compressive strength of the scaffolds. The compressive strength of the scaffolds was between 4.69-9.28

kPa and the 5% $Ba_{0.3}$-BAG+PHBV/PCL scaffold was found to have the maximum compressive strength. In the relative cell viability (%) test, the highest viability was observed on the scaffolds with BAG. The viability changes were very small between groups and contradictory with Ba content for different BAG % groups. It was concluded that PHBV/PCL electrospun scaffold with 5% Ba-BAG has the potential to be used in BTE.

Keywords: Ba doped baghdadite, PHBV/PCL, composite scaffolds, Bone tissue engineering, Electrospinning

ÖZ

KEMİK DOKU MÜHENDİSLİĞİ İÇİN BARYUM KATKILI BAĞDADİT/PHBV LİFLİ İSKELELERİN HAZIRLANMASI

Sadreddini, Sanaossadat
Yüksek Lisans, Biyomedikal Mühendisliği
Tez Yöneticisi: Prof. Dr. Zafer Evis
Ortak Tez Yöneticisi: Prof. Dr. Dilek Keskin

Ocak 2023, 78 sayfa

Son zamanlarda, biyoseramik/polimer kompozitler, kemik dokusu mühendisliği (BTE) kullanarak sert doku hasarını tedavi etmek için çok dikkat çekti. Bu kapsamda, kemik defekti bölgesinde kemik rejenerasyonu sağlayabilen farklı miktarlarda bagdadit (BAG) ve Ba katkılı BAG içeren lifli kompozit PHBV-PCL iskelelerinin geliştirilmesi ve bu iskelelerin yapısal, mekanik ve biyolojik özellikler. BAG ve Ba katkılı BAG sol-jel yöntemi kullanılarak sentezlendi ve 1150°C'de sinterlendi. Mikroyapısal ve biyolojik karakterizasyon sonuçları değerlendirilmiş ve iskele konstrüksiyonları için 4 farklı grup seçilmiştir. Farklı miktarlarda BAG ve Ba katkılı BAG (%1, %3 ve %5 ağırlık) içeren PHBV/PCL kompozit yapı iskeleleri, %72-78 gözeneklilik ile ıslak elektrospinning yöntemiyle üretildi. PHBV iskelelerinde Ba katkılı BAG'nin varlığı, biyoaktivite, hücre canlılığı ve ALP aktivitesinin artmasına neden oldu ve yapı iskelelerinin bozunma hızını kontrol etmek için uygun bir yol getirdi. Yapı iskelelerinde BAG'nin varlığı, yapı iskelelerinin basınç dayanımını iyileştirmiştir. Doku iskelelerin basınç dayanımı 4. 69-9.28 kPa arasında olup, %5 Ba0,3-BAG+PHBV/PCL iskelelerinin en yüksek basınç dayanımına sahip olduğu görülmüştür. Göreceli hücre canlılığı (%) testinde,

en yüksek canlılık BAG'li yapı iskelelerinde gözlendi. Canlılık değişiklikleri, gruplar arasında çok küçüktü ve farklı BAG % grupları için Ba içeriği ile çelişkiliydi. %5 Ba-BAG içeren PHBV/PCL elektrospun iskelesinin BTE'de kullanılma potansiyeline sahip olduğu sonucuna varıldı.

Anahtar Kelimeler: Ba katkılı bagdadit, PHBV/PCL, kompozit yapı iskeleleri, Kemik doku mühendisliği, Elektroeğirme

To my husband and my family

ACKNOWLEDGMENTS

My deepest gratitude is to my supervisor, Prof. Dr. Zafer Evis, and my co-supervisor Prof. Dr. Dilek Keskin for their guidance, criticism, advice, and patience throughout the research.

I would like to extend my sincere thanks to my friends in the laboratory, significantly, Hossein Jodati, Ataollah Nosratinia, İdil Uysal, Engin Pazarçeviren, and Mustafa Nakipoğlu for their help and friendship.

I would like to express my heart-felt gratitude to my family for their unconditional support. For most, I wish to thank my dear husband and my best friend, Amirhossein Fathipour, without whose love, encouragement, and guidance, I would not have finished this thesis.

TABLE OF CONTENTS

LIST OF TABLES

TABLES

LIST OF FIGURES

FIGURES

CHAPTER 1

INTRODUCTION

Bone, a natural biological composite, provides structural and mechanical support, besides flexibility to the body. The unique structure and composition of bone allow it to transform, grow, and repair (Xue et al., 2022). In other words, bone has the ability to regenerate itself. Sometimes, due to trauma, age-related factors, genetics, etc., bone can not go through its natural regeneration process, affecting the patient's quality of life. In these cases, bone tissue engineering plays a vital role in regenerating and reinstructing damaged or lost tissue (Poitout, 2016).

Bone tissue engineering (BTE) combines cells, materials, engineering, and methods to repair and regenerate damaged bone tissue. It is a significant research area that creates implantable bone replacement biomaterials for critical-size bone defects (Poitout, 2016). In order to restore, repair, or regenerate damaged or lost tissues, BTE uses cells, scaffolds, and biological agents like growth factors.

Scaffolds are known as artificial extracellular matrices and have an important role in BTE. They are engineered materials and should have the required properties, such as biocompatibility, bioactivity, and biodegradability, to enhance bone regeneration ability (Popescu and Souto, 2019). Scaffolds need to have properties closely matching the damaged tissue. In order to achieve these properties, suitable biomaterials and fabrication methods should be used (Wu et al., 2017).

The objective of this study was to synthesize Ba-doped BAG and obtain fibrous scaffolds by combining Ba-BAG with PHBV/PCL for having beneficial effects on bone formation, bioactivity, degradation, and mechanical properties for BTE. The effect of Ba-doped BAG on the crystal structure and biological properties pf BAG

was investigated. The PHBV/PCL scaffolds were prepared to contain different amounts of BAG and Ba-doped BAG. The effect of porosity on the mechanical and biological features of scaffolds was investigated. It was assumed that fibrous Ba-BAG+PHBV/PCL scaffolds with high mechanical strength promote cell bioactivity and cell proliferation and osteogenic activity so that they can be used in BTE applications.

CHAPTER 2

LITERATURE REVIEW

2.1 Bone Tissue Engineering

Bone is a living tissue that makes up the skeleton with its own blood vessels and contains various cells, proteins, minerals, and vitamins. It is a natural biological composite with a multi-scale hierarchical structure, high strength, and fracture toughness (Li et al., 2021). This dynamic and integrative tissue provides structural and mechanical support to the body (Lacerda, 2018). The unique structure of bones allows them to grow, transform and self-heal upon bone-damaging conditions caused by trauma, infection, or age-related disease, including fracture and bone defects (Xue et al., 2022). In other words, continuous remodeling of bone guarantees the restoration of bone structure and function over time (Guo et al., 2021).

Despite the spontaneous remodeling and regeneration ability to restore the damaged parts, sometimes bone tissue loss caused by various reasons, including accident trauma, tumor removal, and congenital deformity, can cause challenging clinical problems (Poitout, 2016). Moreover, genetic, age-related factors, etc., prevent bones from repairing the damaged cells, affecting the patient's quality of life (Xue et al., 2022). Tissue engineering (TE) is a promising way to reinstruct and regenerate lost or damaged bone tissues.

TE has attracted attention in science, engineering, medicine, and society since 1980. As Laurencin et al. defined, TE is the application of biological, chemical, and engineering principles toward tissue repair, restoration, and regeneration using cells, scaffolds, and growth factors, alone or combined (Poitout, 2016). BTE uses a combination of cells, materials, and a suitable combination of biochemical and

physiochemical factors to improve or replace biological tissues to restore bone integrity. BTE is an important research area concerned with creating implantable bone replacements for critical-size skeletal defects that cannot heal properly without regenerative approaches. Cells, scaffolds, and growth factors are the key components of BTE. Different strategies have been used in seeding and attaching human cells to scaffolds using various fabrication techniques (Maia et al., 2022).

Mimicking the bone tissue is the main focus of BTE. The bone extracellular matrix is a natural composite containing a polymeric matrix composed mainly of collagen and minerals, mainly calcium phosphate. By considering this complex structure of bone, BTE is trying to develop an improved biodegradable biomaterial (Maia et al., 2022). In this respect, there are two approaches to regenerating the tissue. First, autograph, in which a small number of cells are collected from the patient and seeded to create three-dimensional scaffolds in the presence of growth factors. Under proper conditions, these growth factors will create an actual living tissue in vitro and then be implanted into the patient body to replace the damaged tissue. In the other approach, the scaffold material is implanted directly with or without loading the growth factors into the aimed sites. This approach will guide tissue formation in situ, combined with the degradation of scaffold materials (Poitout, 2016).

According to the latest investigations, the presence of growth factors is not always necessary because, with the presence of bioactive materials, the secretion of growth factors can be induced from host bone cells. It has been agreed that scaffolds are the most important issue in the TE field. Still, the sensitive and complex system of the human body makes selecting the scaffold materials strict and extremely challenging (Poitout, 2016).

Being biocompatible and non-toxic are the basic requirements in selecting materials for a scaffold. The scaffold should not induce any foreign body reactions. Biodegradability is another requirement and the degradation/absorption rate should match the tissue growth. Moreover, the material's mechanical properties should match the biological tissue to provide good support until the new tissue can support itself (Poitout, 2016). When the mechanical properties of scaffolds match perfectly

or very closely with the biological tissue, the chance of the body accepting the scaffold and promoting new tissue is higher. So the properties close to the bone will benefit the bone scaffold (Wu et al., 2020). Finally, the materials should promote cell growth, differentiation, and tissue regeneration. They should also support angiogenesis, so the vessels can transport nutrients and oxygen to the developing tissue and remove waste (Wu et al., 2020). Thus the ideal scaffold should also have a suitable porosity and pore size range (Pore size of at least 10 μm (Wu et al., 2020)).

Autograft and allograft are the two traditional ways to regenerate and treat damaged tissue. But these costly procedures have limited clinical success due to their clinical complications, such as risks of infection and rejection. Therefore the clinical demand to create safe, reliable, and cost-effective alternatives increases (Wu et al., 2020). Materials used for bone tissue engineering include natural polymers (such as collagen, fibroin, etc.) and synthetic ones (polycaprolactone, poly lactic-co-glycolic acid, etc.). Recently, synthetic materials have driven huge attention. Ceramics, polymers, and composites have been investigated as scaffold materials for BTE.

2.2 Scaffolds

With the growing elderly population and increasing bone-related diseases, the health system's main concern is solving the transplant crises (Donnaloja et al., 2020). The lack of suitable donors for transplants has increased the need for designing cost-effective alternatives for restoring tissue function (Popescu and Souto, 2019). Developing a biomaterial with similar characteristics to biological bone tissue is challenging, and it is one of the most exploited fields in BTE. BTE combines concepts from engineering and biology by using the human body’s potential to repair or create tissue (Popescu and Souto, 2019). The developed biomaterials should provide mechanical support and osteoconduction, and subsequently, they should fuse with natural bone tissue. In addition, these biomaterials should facilitate rapid bone regeneration by recruiting stem cells by releasing bioactive molecules.

The important factors associated with scaffolds are biocompatibility, biodegradability, porosity, suitable mechanical properties, and cell attachment (Lacerda, 2018; Wu et al., 2020). They should be able to provide the needed space for the newly formed bone (Popescu and Souto, 2019).

The biological extracellular matrix is porous and is composed of a mixture of complex proteins and growth factors. This complex structure provides suitable biological, chemical, and physical parameters to direct cellular activity. So, a scaffold should be able to provide characteristics similar to native bone structures. Surface roughness, porosity and pore size, degradation, mechanical properties, biocompatibility, and interconnectivity, are the most important characteristics that should be considered for bone scaffolds (Perić Kačarević et al., 2020). Generally, a functional microenvironment for cellular adhesion, growth, and spreading should be provided by a scaffold. The microstructure of a scaffold, including porosity, pore size, and interconnectivity between pores, is very important for ensuring cell survival because it should provide a correct transmission of nutrients, oxygen, and wastes (Perić Kačarević et al., 2020; Popescu and Souto, 2019). To be summarized, an ideal scaffold should fulfill the following criteria. First, its structure should be as close as possible to the implanted tissue. Second, it should be biocompatible and biodegradable. Third, the surface of the scaffold should be capable of promoting the adhesion, proliferation, and differentiation of stem cells (Boccaccio, 2021).

2.2.1 Materials for Scaffolds

The mentioned factors are the main reasons that, nowadays, a vast effort has been spent searching for an optimal material with the required properties. To achieve these qualities, various scaffolds have been prepared by using a massive variety of materials, each for a unique purpose, so different perspectives of these materials have been analyzed, from biocompatibility to the ideal 3D bone-like architectural structure (Donnaloja et al., 2020). For developing a customized scaffold, materials and performance are two important factors (Wu et al., 2017). Scaffolds are generally

made from either biological or synthetic polymers, bioactive ceramics, glasses, metals, or composites (Stevens, 2008).

2.2.1.1 Biological Materials

Biological polymers mainly involve proteins such as collagen, gelatin, silk and polysaccharides such as hyaluronic acid, alginate, and cellulose, which are appropriate candidates for BTE. They contain biofunctional molecules, which result in the ability to remodel naturally (Donnaloja et al., 2020). They can provide innate biological guidance to cells that favor cell attachment and promote chemotactic responses. Having the mentioned advantages, there are still some concerns limiting the usage, like the potential risk of disease transition because of microbial continence and immunogenic responses, uncontrolled biodegradation rates, and weak mechanical properties (Perić Kačarević et al., 2020; Stevens, 2008).

Collagen is one of the most studied natural polymers for biomedical applications, which is the basic component of several animal tissues, presenting a good binding site for bone cell adhesion (Donnaloja et al., 2020). This biological polymer contains advantages such as cytocompatibility, similarity to extracellular matrix, biodegradability, and ability to possess different physical forms. On the other hand, low mechanical strength, difficult disinfection, and difficult handling are disadvantages that limit their use as implant materials. Several kinds of researches have been tried to overcome these problems such as using collagen as the minor component in the scaffold (doping collagen with hydroxyapatite). Another strategy is the addition of an inorganic element to the structure to overcome the poor mechanical properties (Donnaloja et al., 2020). Gelatin is a very compatible and biodegradable natural polymer that has the ability to adjust the pore size, but it has poor mechanical properties and low stability in physiological conditions (Alipal et al., 2019).

2.2.1.2 Synthetic Materials

Some polymers are synthesized under controlled conditions and have more predictable and reproducible final forms that make their mechanical and physical properties more controllable, and they do not pose immunogenic risks (Perić Kačarević et al., 2020; Stevens, 2008). Their degradation rate can be altered by changing their chemical composition, crystal structure, and molecular weight. Compared with natural polymers, they have a low bioactivity rate on the surface. Poly (3-caprolactone) (PCL), polylactic acid (PLA), polyglycolic acid (PGL), and poly-lactic-co-glycolide (PLGA) are examples of synthetic polymers.

One of the most often employed synthetic polymers in the BTE is PCL, which has a semi-crystalline structure. Being non-toxic and having a low degradability rate makes PCL a good choice for load-bearing applications. PCL has low bioactivity and a hydrophobic structure that can cause problems in cell adhesion, and these factors limit the usage of PCL. Co-polymerization of PCL is an approved strategy to overcome this problem, and it's been indicated that this strategy can remarkably increase bioactivity, too (Donnaloja et al., 2020).

PLA is another synthetic polymer that has been involved in most researches related to the bone tissue regeneration field. It is characterized by properties fundamental for bone regeneration, including degradability, non-toxicity, thermal stability, and compatibility (Gregor et al., 2017). The co-polymer of PLA with PGA is polylactic co-glycolide (PGLA), is another widely used synthetic polymer, and it is preferred due to its degradation rate, but its mechanical properties limit its usage in load-bearing applications (Donnaloja et al., 2020).

2.2.1.3 Bioceramics

In recent decades, researchers have been trying to introduce new advanced biomaterials to the medical field for skeletal repair and regeneration, which include a combination of ceramics referred to as "bioceramics" (Zafar et al., 2019).

Bioceramics were highly investigated in BTE due to their biocompatibility, bioactivity, osteoconductivity, and mechanical strength. They have the ability to promote the formation of new bone. Calcium phosphate and calcium sulfates are the most commonly used bioceramics. Calcium phosphates have been used extensively in BTE due to their similarity to bone minerals. Hydroxyapatite (HA), tricalcium phosphate (TCP), and biphasic calcium phosphate are the most researched calcium phosphates (Perić Kačarević et al., 2020). HA (which is the main mineral component of natural bone) has low resorption and remodeling rate, so it cannot be used in all BTE applications. TCP has a higher resorption rate than HA, thus, degrading faster. So by combining these two elements, an ideal resorption and degradability rate for BTE can be achieved (Perić Kačarević et al., 2020).

Since bioceramics have similar physiochemical characteristics to damaged hard tissues, as was previously indicated, they have been extensively used in the BTE sector for many years to restore or replace these tissues. These researches aim to develop an ideal scaffold that enables new bone formation and provides the necessary properties such as porosity, bioactivity, biocompatibility, and mechanical strength. Bioactive ceramics such as TCP, HA, and β-TCP/HA can provide suitable mechanical stability when they bind to hard tissues and have the ability to create porous scaffolds. Still, they are brittle and difficult to form complex shapes (Roohani-Esfahani et al., 2012).

Among bioactive ceramics, calcium-silicate-based bioceramics have shown great bioactivity and biodegradability with a suitable rate for bone regeneration, but like other bioceramics, they are brittle, and they own low strength, but more importantly, calcium-silicate based bioceramics have high dissolution rate (Jodati et al., 2020; Wu and Chang, 2013). Besides the disadvantages mentioned, the major drawback of Ca-Si-based bioceramics is their chemical instability (Roohani-Esfahani et al., 2012). Addition of a third component, such as Zirconium (Zr), Zinc (Zn), and Magnesium (Mg), to the structure of calcium-silicate-based bioceramics, is a promising path to overcome the disadvantages and improve and control the mechanical properties, stability, and bioactivity (Wang et al., 2014).

2.2.1.4 Bioactive Glasses

Bioactive glasses are amorphous solid silica-based materials with high biocompatibility and the ability to bond with soft and hard tissues. According to research, they have the ability to stimulate more bone regeneration compared with bioceramics (Daskalakis, 2021; Jones, 2015). Studies on bioglasses have shown that they permit direct bonding between their surfaces and surrounding living tissues. Bioglasses' composition and surface area depend on morphology and particle size, so a slight change in these factors can affect the degradation rate (Daskalakis, 2021). Using this property, Larry L. Hench invented the first bioactive glass in 1969 (Jones, 2015) called 45S5, satisfying 45 wt% SiO_2 and a 5 to 1 ratio of CaO to P_2O_5. They showed that slightly changing the composition of bioglasses can define their bioactivity, bioinertness, and resorbable properties.

Different materials and synthesizing methods can control and improve the bioactivity and resorption rate. Due to low mechanical strength and fracture toughness, sometimes, there are limitations in using bioglasses in load-bearing applications.

2.2.1.5 Composites

A composite material is a bioactive material produced from two or more constituent materials with different physical and chemical properties. It can be assumed that composites are effective tools for overcoming the disadvantages of other biomaterials (Maia et al., 2022). The newly formed materials usually have different characteristics owing to the properties of their ingredients. The most significant advantage of composites is their high strength-to-weight ratio. These materials aim to mimic the structural properties of natural bone (Stevens, 2008). Composites are usually classified into three main groups based on the materials used in their matrix: polymer-based matrix, ceramic-based matrix, and metal-based matrix. The properties of composites vary with changing the materials used for synthesizing. The

most commonly used composites are polymer-based matrices. These polymeric base composites are usually combined with bioactive ceramic particles (Martel and Olivas-armendariz, 2016).

2.2.2 Use of Metal Dopants

Polymers and ceramics have been used extensively in BTE, but their weak mechanical properties raise questions about whether they are suitable or not. Metallic biomaterials with acceptable biocompatibility (Biometals) have high mechanical strength and elasticity, making them ideal for bone tissue replacement. Stainless steel, silver, and aluminum are examples of metals that have been used in the history of BTE because of their excellent mechanical strength, fatigue resistance, and good act in load-bearing applications. Most of these biometals are non-degradable, which makes the need for a second surgery to remove the implant necessary. In some cases, it remains in the patient body for a lifetime. Nowadays, in the field of BTE, some degradable metals such as Mg and Fe are being used, and they have mechanical properties similar to natural bone tissue. But metallic ions are being released from these materials, which could be harmful. The other problem with these materials is their unsuitable degradation rate. Fe has a low degradation rate, and in the case of Mg, it has a high degradation rate. Alloying these biometals with ions like calcium or strontium can be beneficial for controlling the degradation rate (Perić Kačarević et al., 2020).

2.2.3 Fabrication Methods

The success of a scaffold can also be related to the design and manufacturing of the scaffold. In order to make the scaffolds suitable and implantable in the body and based on the biomaterials of the scaffold, different fabrication methods can be used. These methods should be able to guarantee micro and macro-structural properties. The fabrication method should not change the chemical properties and

biocompatibility of the material (Jokanović et al., 2019). Solvent casting and particle leaching, gas-foaming, phase separation, electrospinning, and sol-gel, are the conventional methods for scaffold manufacturing. Selecting the fabrication method is challenging, and it should be able to keep the mechanical and bioactivity properties. Generally it is known that properties such as porosity and mechanical strength are influenced by the fabrication method (Perić Kačarević et al., 2020).

2.2.3.1 Solvent Casting and Particle Leaching

The solvent casting method (Figure 2.1) is a manufacturing process used to produce flexible plastic components. In this method, solvent casting and particle leaching, an organic solvent is used to dissolve the polymer with the leaching materials (salt or sugar-like molecules, which will not get dissolved in the organic solvent) followed by casting of the mixture into a mold, then the drying salt like particles was leached by evaporating the water. Finally, the polymer particles will create a porous structure (Jokanović et al., 2019). This method is cost-effective and simple and allows controlling the porous size. Also, this method allows the preparation of scaffolds with normal porosity, but it has two main disadvantages. First, the solvent should be evaporated to avoid the seeding of possible proteins or other active molecules (which have built-in the solvent). Second, the agglomeration of salts results in an uneven distribution of scaffold pores (Jokanović et al., 2019; Sachlos et al., 2003). This method comes with other disadvantages, such as cytotoxicity, poor interconnectivity, and a lack of control over the spatial geometry.

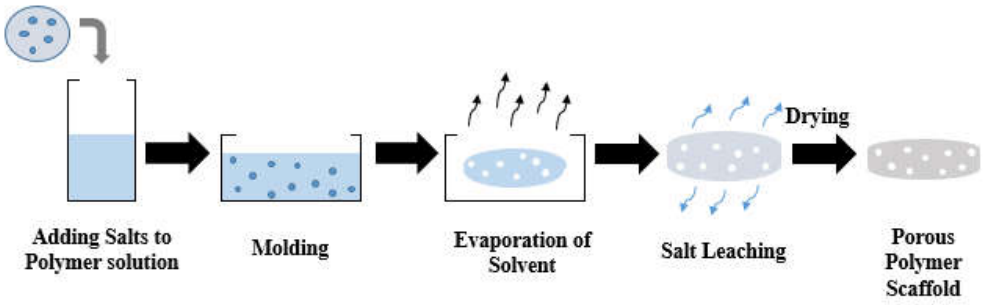

Figure 2.1. Solvent casting and particle leaching method

2.2.3.2 Gas-Foaming

In the gas-foaming method (Figure 2.2), CO_2, N_2, or He is used. In this method, the polymer discs are placed on lattice plates and exposed to high-pressure gas (CO_2 is the most commonly used due to its low toxic, non-flammable, stable, inexpensive, and environmentally acceptable properties (Jokanović et al., 2019)). This high pressure will result in forming of bubbles inside the polymer structure. Then the pressure will slowly be decreased to the atmosphere level, and the gas is going to be released by reducing its solubility in the polymer. Escaping the gas will result in the formation of pores in the scaffold. This method is suitable for types of scaffolds that are sensitive to solvent (The solvent is not organic) and high temperatures (Guo et al., 2021; Perić Kačarević et al., 2020). In this method, factors such as the concentration of gas in the polymer, pressure, temperature, soaking time, the chemical composition of the polymer, etc., will significantly affect the size of the pores. Reports have shown that rapid gas release will result in smaller pores; conversely, a slow release will result in bigger pore size (Poitout, 2016). This technique is fast and simple, but the pores lack interconnectivity.

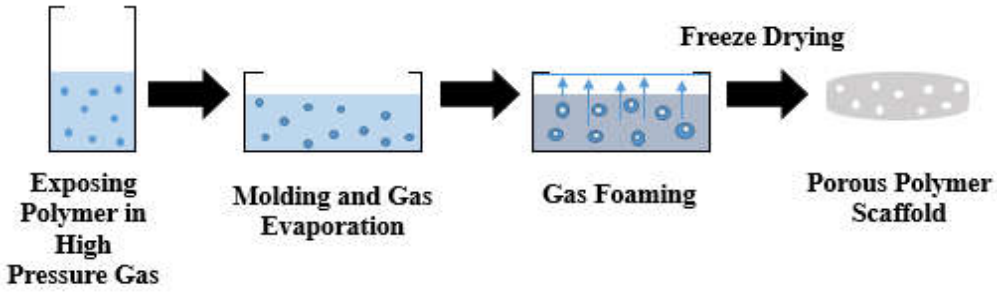

Figure 2.2. Gas-foaming method

2.2.3.3 Phase Separation

In the phase separation method (Figure 2.3), a solvent with a low melting point is used to dissolve the polymer. Then water is added to the solution to create two aqueous and organic phases. This separation includes the presence of polymer in large quantities in one phase and a small amount in the other phase. At this point, the

temperature will decrease below the melting point of the solvent until the mixture becomes solid, followed by the removal of the low-content phase from the polymer. After drying with a vacuum, a pores scaffold will be obtained. This method results in high interconnectivity of pores, but the obtained pore size with this method is limited (Guo et al., 2021; Jokanović et al., 2019).

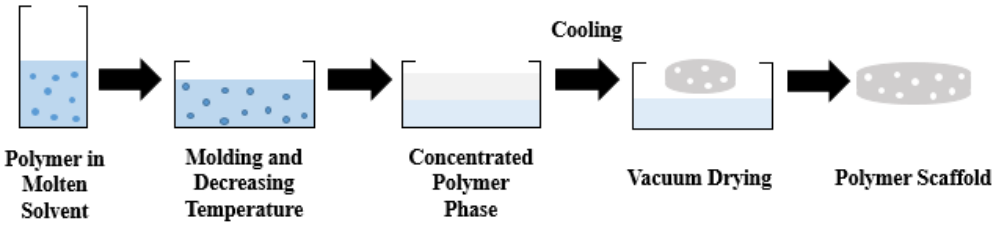

Figure 2.3. Phase separation method

2.2.3.4 Electrospinning

Electrospinning is the most widely used method for fabricating nanofibrous scaffolds. In this method (Figure 2.4), a solvent will dissolve the polymer, and then the mixture will be poured into a syringe. Using mechanical pressure and high voltage electrical field, the polymer will eject continuously, and while the solvent is evaporating, the solid polymer will be collected by a dry or wet collector. Stacking polymer fibers in a continuing way will result in the formation of porous scaffolds. In this method, pore size is controllable by changing the current, flow rate, distance of syringe and collector, and voltage (Guo et al., 2021).

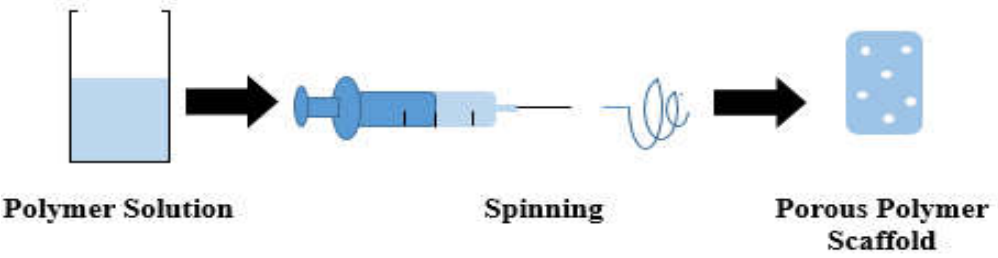

Figure 2.4. Electrospinning method

2.2.3.5 Sol-Gel

The sol-gel method involves gel foaming with the help of surfactants. In this method, the solution will undergo a condensation and gelation process at room temperature. Following drying and heating. And finally, after the removal of the liquid, the product will be sintered. The scaffolds produced with this method will have high porosity but low mechanical strength, which can be solved using polymer coating (Daskalakis, 2021).

2.2.3.6 Freeze Drying

In the freeze-drying method, a porous scaffold is obtained by lowering the temperature and pressure. In this method, the temperature of the solution is decreased (below freezing point), then the frozen liquid is removed by vacuum (sublimation) (Figure 2.5). The size of pores can be controlled by the freezing rate (a slow freezing rate produces bigger pores) (Sachlos et al., 2003).

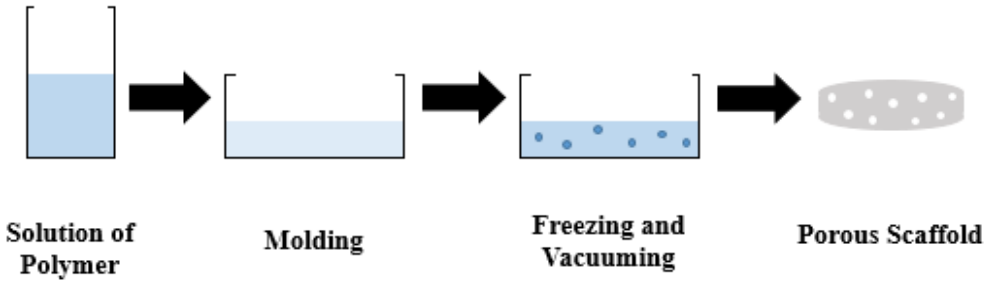

Figure 2.5. Freeze drying method

2.3 Materials Used in BTE Scaffolds Developed in the Thesis

2.3.1 Baghdadite

Baghdadite ($Ca_3ZrSi_2O_9$), a calcium-silicate-based bioceramic with zirconium in its structure, was first discovered in Qala-Deniz, NE, Iraq, and is named after Baghdad (Al-Hermezi et al., 1986).

2.3.1.1 Structure of Baghdadite

Natural BAG is a very rare biomaterial and is a calcium-silicate bioceramic with Zr in its structure. It is characterized by the presence of walls of cation polyhedral, which are linked together by direct connection and disilicate groups. BAG's general formula is M_4 (Si_2O_7) X_2, where M is a cation with various charges and ionic radiation (Biagioni et al., 2010). Zirconium is biocompatible, and its mechanical properties for bone and dental applications are quite suitable (Kosmač and Kocjan, 2012; Piconi and Maccauro, 1999). Zirconium can create a network that allows it to bind to Ca ions ionically, and this binding enables the formation of BAG with improved stability (Jodati et al., 2020).

Natural BAG is colorless, transparent, and does not tend to conchoidal fracture (Al-Hermezi et al., 1986). The crystal structure of natural BAG is monoclinic with space group $P2_1/c$, according to data from x-ray powder diffraction, and the unit cell parameters of this rare natural bioceramic are described as a=7.36Å, b=10.17Å, c=10.45Å, α=90°, β=90.87°, γ=90°. The calculated density for BAG is 3.49 g/cm^3, with a volume cell of 782.72 (10^6pm^3)Å^3.

2.3.1.2 Properties of Baghdadite

(Roohani-Esfahani et al., 2012) were the first researchers that develop a BAG base porous scaffold, with and without surface modification with PCL in a way that was

suitable to use for critical-sized bone defects, and tested it on a rabbit radius under normal load. According to the radio-graphical images of this test, there was better bone growth after 12 weeks of BAG scaffold implantation than (TCP)/HA scaffolds (Jodati et al., 2020; Roohani-Esfahani et al., 2012). But despite these promising results, the unmodified BAG scaffold was not completely suitable for load-bearing bone defects when exposed to high compressive stresses.

(Li et al., 2016) tested a modified and unmodified BAG scaffold on sheep tibiae. To avoid stress-related problems, surface modification with a thin layer of PCL was used as a coating in this experiment. This modified BAG scaffold had improved mechanical strength and toughness, and the fracture behavior of this scaffold decreased as expected. So from this test, it could be concluded that both modified and unmodified BAG scaffolds have improved mechanical and biological properties. They can help bone regeneration even in the absence of cells or bioactive molecules. Still, modified scaffolds of BAG can decrease the risk of failure and inflammatory reactions because they decrease the brittleness properties (Li et al., 2016).

Structural properties of the BAG scaffolds were characterized by various tests including x-ray diffraction (XRD), scanning electron microscope (SEM), furrier transform infrared spectroscopy (FTIR), transmission electron microscopy (TEM), etc. The result of the mentioned tests showed that, due to the presence of Zr in the structure of BAG scaffolds, they possess higher mechanical and biological properties in comparison with HA. The tests also revealed that BAG scaffolds have similar porosity properties (size and interconnectivity) to the natural bone, facilitating blood circulation, and no cytotoxicity effects were observed. These two qualities result in cell growth, better cell attachment and proliferation on the surface of the scaffold, and finally, better formation of bone tissues (Arefpour et al., 2020, 2019).

According to the porosity and compressive strength measurements, higher porosity will result in lower compressive strength. Considering this, BAG scaffolds still didn’t have the compressive strength similar to natural bone. So in order to improve the compressive strength, PCL was used as a coating polymer due to its high toughness, biocompatibility, and biodegradability. PCL coating increases strain to

failure by filling and clogging some pores, which leads to decreased brittleness and improves BAG strength. Comparing the PCL-coated BAG scaffold with the BAG scaffold showed higher compressive strength in scaffolds upon PCL coating (Arefpour et al., 2020, 2019). When compared to HA and -TCP, BAG scaffolds demonstrated superior cell adhesion, proliferation, and differentiation into cementogenic and osteogenic cells. (Jodati et al., 2020).

2.3.1.3 Drug Release and Antibacterial Properties of BAG

Sehgal et al. (Sehgal et al., 2017) fabricated a porous BAG structure coated with dexamethasone disodium phosphate (DXP) using the sponge template method to develop a bioactive scaffold with the ability to sustain delivery of the osteoinductive drug. In vitro studies were carried out to validate the regulated release of osteogenic stimuli. The osteogenic differentiation of MG 63 cells on BAG scaffolds with DXP-encapsulated chitosan nanoparticles as a coating was significantly higher than that of MG 63 cells on uncoated BAG scaffolds as a result of the regulated distribution of DXP from the scaffolds to the cells. Moreover, the antibacterial activity of 1, 3, and 5 wt% vancomycin-loaded BAG scaffolds against *Staphylococcus aureus* was documented by (Bakhsheshi-Rad et al., 2017). The findings showed that the antibacterial properties of vancomycin-loaded BAG scaffolds considerably decreased the post-surgery infection risks, which are a main cause of therapeutic failure for bone abnormalities.

2.3.1.4 Bioactivity and Degradability of BAG

Prior to in vivo research, apatite formation on the surface of various materials submerged in simulated body fluid (SBF) for a predetermined amount of time has been used to predict material bonding ability to surrounding host bone tissue. (Bohner and Lemaitre, 2009). As (Kokubo and Takadama, 2006) reviewed a pattern that showed SBF could be used to test bioactivity. To avoid the early precipitation

of HA, (Bohner and Lemaitre, 2009) suggested a method upgrade that makes use of dual solutions. Since then, a significant increase in the number of research reporting BAG's bioactivity was seen. (Jodati et al., 2020).

The performance of scaffolds is greatly influenced by the biodegradability rate, particularly in load-bearing applications. A balance between the implant's degradation rate and the pace at which new bone tissue regenerates should be reached in order to gradually transfer the load from the implanted scaffold to the newly created bone tissue and to prevent implant failure. When assessing the in vitro degradation of scaffolds after weight loss, buffers like phosphate buffer solution (PBS) or SBF are used as a function of immersion time. BAG has an extremely high rate of deterioration, according to reports (Jodati et al., 2020).

2.3.1.5 Mechanical Properties of Baghdadite

The effect of BAG on the mechanical properties of scaffolds has been investigated in many studies. A study by (Samani et al., 2019) shows that adding less than 5 wt. % BAG to the PCL/graphene scaffold enhanced the fracture strength and elastic modulus up to 61% and 330%, respectively. In a study by (Abbasian et al., 2020) it has been reported that adding BAG to the nylon6 increased both compression strength and compression modulus because BAG addition reduced the porosity of the nanocomposite scaffold. The reverse relationship of porosity and mechanical properties of BAG scaffolds was investigated by (Sadeghpour et al., 2014). In the mentioned study, the freeze casting method was used to produce BAG-based scaffolds, and the main focus was the mechanical properties and porosity and their relations with cooling rate and solid loading. As expected, the mechanical properties and porosity had inverse relationship. On the other hand, higher cooling rates resulted in enhanced mechanical properties.

Porosity-stiffness relations play an important role in the design of scaffolds for BTE.

In a study by (Sadeghzade et al., 2019) the effect of sintering temperature on the BAG scaffolds was evaluated, and as expected, as the temperature increases, the compressive strength and modulus of the scaffolds increase as well. Also, some other studies (Roohani-Esfahani et al., 2012) observed enhanced mechanical properties for BAG scaffolds when polymeric materials were used as coating scaffolds.

2.4 Poly (hydroxybutyrate) co-(hydroxyvalerate) (PHBV)

As mentioned before, biodegradable and biocompatible polymers have been used widely in BTE applications. Polyhydroxyalkanoate (PHA) is a biopolymer synthesized by microorganisms such as soil bacteria and genetically modified plants (Sombatmankhong et al., 2007). PHA is a microbial polymer of hydroxyl derivatives of fatty acids and is highly biocompatible and biodegradable. PHA has various monomers resulting in a variety of physiochemical properties. For example, the homopolymer of PHA, known as polyhydroxy butyrate (PHB), has very high crystallinity (about 70%), and products produced from this polymer are rigid and porous (Anatoly N. Boyandina and Sukovatiya, 2016). Poly (hydroxy valerate) (PHV) is another example of a commonly used member of PHA because of its possibility for tailoring the physical characteristics (Sombatmankhong et al., 2007). Poly (3-hydroxybutyrate-co-2-hydroxy valerate) or PHBV, is the copolymer of PHB and PHV and is the most commonly used member of PHA polymers. Its crystallinity varies between 50-70% (Ibrahim et al., 2021).

PHBV is a biocompatible, biodegradable, and non-antigenic co-polymer, which has attracted attention as a potential scaffold material for BTE applications (Lü et al., 2012). PHBV is known for its three main features: biocompatibility, biodegradability, and being a biobased polymer, meaning that its synthesis starts from renewable resources. These three features of PHBV qualify it as a good candidate to replace conventional non-degradable polymers. Also, PHBV has shown great biocompatibility, biodegradability, and flexibility in BTE applications. Its weak mechanical properties, low thermal stability, difficult processability, and

considerable hydrophobicity are the main drawbacks limiting this polymer's usage area. Much research has been focused on overcoming the disadvantages of PHBV and producing PHBV-based materials with desirable properties (Ibrahim et al., 2021).

PHBV chain's flexibility increases by incorporating PHV into the PHB main chains. Therefore a decrease in melting temperature and glass transition and an increase in processability are observed. The in vitro biocompatibility studies of PHBV fabricated by various methods, including solvent casting and particle leaching technique, showed a good adhesion of cells on the surface of PHBV films, which suggested a high possibility of developing PHBV as a tissue scaffold. The properties of PHB and PHBV films were proved to be similar, but due to the fragility of PHB, the potential use of PHB is limited. So, co-polymerization with a flexible co-monomer, PHV, can optimize the properties (Sombatmankhong et al., 2007).

2.5 Aim of the Study

The current research aims to develop baghdadite/PHBV scaffolds using Ba^{2+} doped baghdadite and investigate its properties as a new biodegradable and bioactive BTE scaffold. In this study, Ba was doped to baghdadite and then incorporated into PHBV fibers during electrospinning for the first time.

The specific objectives are summarized as follows:

1. Synthesize pure and Ba^{2+} doped baghdadite using the sol-gel method and characterizing via XRD, FTIR, SEM, ICP, and cytotoxicity assays.
2. Preparing baghdadite/PHBV scaffolds with different BAG amounts using electrospinning. Evaluating the prepared scaffolds by SEM, degradation, bioactivity, porosity density, viability, ALP analysis, and mechanical tests.

The schematic illustration of the electrospinning systems of the scaffold is presented in Figure 2.6.

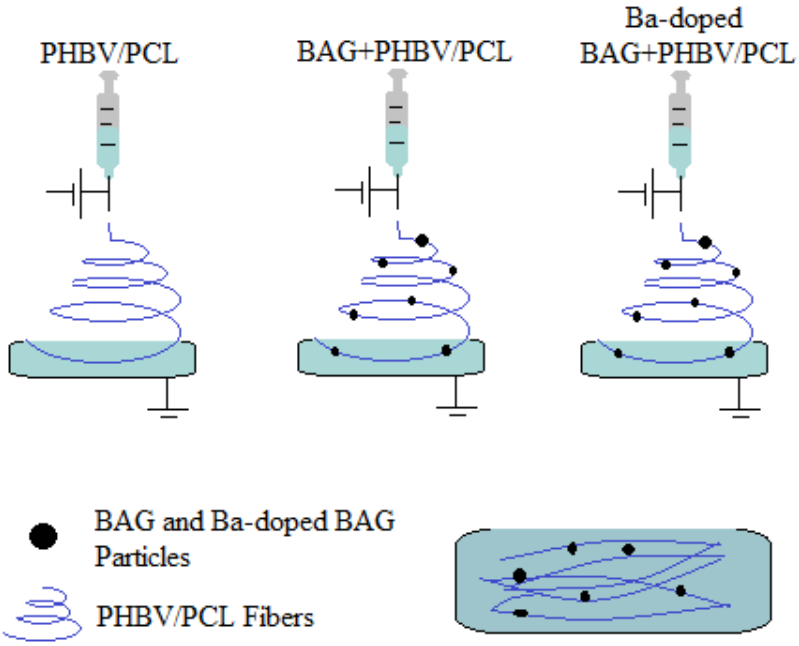

Figure 2.6. Schematic illustration of electrospinning systems of scaffold

CHAPTER 3

MATERIALS AND METHODS

3.1 Materials

For synthesizing pure baghdadite, calcium nitrate tetrahydrate ($Ca(NO_3)_2.4H_2O$) (Merck, Germany), zirconium (IV) oxynitrate hydrate ($N_2O_7Zr.xH_2O$) (99%, Sigma Aldrich, USA), tetraethyl orthosilicate($C_8H_{20}O_4Si$) (Reagent grade, 98%, Sigma Aldrich, China), ethanol absolute (C_2H_6O) (Isolab, Germany), and nitric acid (HNO_3) (65%, Isolab, Germany), were used. For Ba^{2+} doped samples, an additional compound, barium nitrate ($Ba(NO_3)_2$) (99%, Sigma Aldrich, India), was used besides these chemicals.

Poly(3-hydroxy butyric acid-co-3-hydroxy valeric acid) (PHBV) (Sigma Aldrich, USA), polycaprolactone $(C_6H_{10}O_2)_n$ (Mn=80000, Sigma Aldrich, Japan), and ethanol (C_2H_6O) (Isolab, Germany) were used to synthesize fibrous scaffolds using electrospinning method.

Sodium chloride (NaCl) (Isolab, Germany), potassium chloride (KCl) (Merck, Germany), disodium hydrogen phosphate anhydrous (Na_2HPO_4) (Applichem Panreac), potassium dihydrogen phosphate (KH_2PO_4) (Merck, Germany), hydrochloric acid 37% (HCl) (Merck, Germany), Sodium hydrogen carbonate ($NaHCO_3$) (Riedel-deHaen, Eur), di-potassium hydrogen phosphate trihydrate ($K_2HPO_4.3H_2O$) (Merck, Germany), magnesium chloride hexahydrate ($MgCl_2.6H_2O$) (Merck, Germany), calcium chloride ($CaCl_2$) (Merck, Germany), sodium sulfate anhydrous (Na_2SO_4) (Riedel-deHaen, Eur), Tris (Hydroxymethyl) aminomethane ($H_2NC(CH_2OH)_3$ (Merck, Germany), were used for the preparation of PBS and SBF solutions.

For cell culture studies, DMEM high glucose (BI), foetal bovine serum (BI), pen-strep solution (BI), sodium pyruvate solution (BI), trypsin EDTA solution A (BI), trypan blue 0.5% solution (BI), sodium carbonate (Na_2CO_3) (Merck, Germany), sodium bicarbonate ($NaHCO_3$) (Sigma Aldrich, USA), triton X-100 (Sigma Aldrich, USA), PNPP (Sigma Aldrich, USA), cupric sulfate pentahydrate ($CuSO_4*5H_2O$) (Sigma Aldrich, USA), bicinchoninic acid (BCA reagent) (Sigma Aldrich, USA), ascorbic acid (Sigma Aldrich, USA), β-glycerophosphate (Sigma Aldrich, USA), dexamethasone (Sigma Aldrich, USA), o-cresophthalein (Merck, USA), 8-hydroxyquinone-5-sulfonic acid (Merck, USA), ethanolamine (Acros), and Alamar Blue (Invitrogen, USA) were used.

3.2 Methods

3.2.1 Synthesis and Characterization of BAG and Ba-Doped Baghdadite

3.2.1.1 Synthesis of Ba-doped BAG

BAG and Barium-doped baghdadite were synthesized using the sol-gel method. For synthesizing a BAG using the sol-gel method, calcium nitrate tetrahydrate ($Ca(NO_3).4H_2O$), zirconium (IV) oxynitrate hydrate ($N_2O_7Zr.xH_2O$), and tetraethyl orthosilicate ($C_8H_{20}O_4Si$) were used as precursors. First, tetraethyl orthosilicate (TEOS)(4.55 mL), Nitric acid 2M (1 mL), and absolute ethanol (50 mL) were mixed and stirred for one and half hours at room temperature (Nitric acid was added to the solution for hydrolyzing TEOS). Meanwhile, zirconium (IV) oxynitrate hydrate (2.335 g) and absolute ethanol solution (50 mL) was stirred for 2 h at room temperature. Then calcium nitrate tetrahydrate (7.084 g) and prepared Teos solution was added to Zr solution and stirred at room temperature for 5 h. Then all the clear solutions were dried at 60 °C for 24 h and again at 90 °C for another 24 h. Finally, the dried solution was sintered at 1150 °C for 3 h to obtain a fine BAG.

For synthesizing a fine Ba-doped BAG using the sol-gel method, the same materials and barium nitrate were used as precursors. First, barium nitrate (0.196g, 0.392g, and 0.784g to obtain $Ba_{0.075}$, $Ba_{0.15}$, and $Ba_{0.3}$, respectively) was stirred with nitric acid 2 (1mL) molars for 1h. Then it was added to TEOS (4.55 mL) and absolute ethanol (50 mL) and mixed and stirred for one and half hours at room temperature (Nitric acid was added to the solution to help dissolve barium nitrate and hydrolyzing TEOS). Then the solution was added to zirconium (IV) oxynitrate hydrate (2.335 g) and absolute ethanol solution (50 mL), which also was stirred for 2 hours at room temperature. Following the addition of calcium nitrate tetrahydrate (6.888g, 6.692g, and 6.3g respectively) and stirring for 5 h. Finally, the solution was dried at 60°C for 24 h, and again at 90°C for another 24 h, and to further remove the water, it was sintered at 1150° C for 3 h.

The amount of the elements used to prepare pure and Ba-doped BAGs at different ratios is shown in Table 3.1.

Table 3.1 Molar concentration of the elements used in the preparation of pure and doped BAGs.

Sample	Ca	Zr	Si	Ba
BAG	3	1	2	0
$Ba_{0.075}$-BAG	2.925	1	2	0.075
$Ba_{0.15}$-BAG	2.85	1	2	0.15
$Ba_{0.3}$-BAG	2.7	1	2	0.3

3.2.1.2 Structural Characterization of BAG and Ba-Doped BAG

3.2.1.2.1 X-ray Diffraction (XRD) Analysis

To identify the crystal structure of the synthesized samples, X-ray diffraction analysis was performed using a Rigaku Ultima IV X-ray diffractometer in the Central

Lab, METU, operated at 40 kV and 30 mA, with monochromic Cu-Kα radiation with a wavelength of 0.1506 nm. All patterns were collected with 2θ angles of 10° to 70° with step size 0.1°. To analyze the peaks, Joint Committee on Powder Diffraction Standard (JCPDS) files were used to compare. The average crystal size of the samples was calculated using full wide at half minimum (FWHM) and Scherrer's formula (Equation 3.1).

$$D = K\lambda/\beta \cos\theta \quad (3.1)$$

This formula is known as the Scherrer equation, where:

D=Crystal (Grain) size (nm)

K=Scherrer constant, which varies with the habit, and it is agreed to be 0.9

λ=Wavelength of the XRD sources (0.1506 nm)

β=FWHM (Radians)

θ=Diffraction angle of the sample (Radians).

The crystallite degree was calculated using Equation 3.2. In this equation, the area of crystalline peaks and the area of all mountains have been found using Origin Lab Software.

$$Crystallinity\ degree = \frac{Area\ of\ crystalline\ peaks}{Area\ of\ all\ peaks} \times 100 \quad (3.2)$$

Finally, lattice parameters and cell volume were calculated using Unit Cell Software of Holland and Redfern via refinement driven out of XRD data.

3.2.1.2.2 Fourier Transform Infrared Spectroscopy (FTIR)

To highlight the functional groups in samples, FTIR was used. Through the use of 100 scans on a Bruker IFS 66/S spectrometer in the Central Lab at METU, the spectrum was captured between 4000-400 cm^{-1}.

3.2.1.2.3 Scanning Electron Microscopy (SEM)

In the Central Lab, METU, SEM analysis was carried out using a QUANTA 400F Field Emission SEM equipment with a resolution of 1.2 nm to examine the shape and grain size of pure and doped baghdadite particles. To have better results, instead of using dry samples powder, samples were poured into an insoluble liquid, in this case, ethanol. Then particles of samples dispersed and got smaller using an ultrasonic probe. Finally, the prepared new samples were dropped on aluminum sheets and attached to metal stubs using carbon tape. After drying (for a couple of minutes at room temperature), samples were vacuum coated with gold using the Hummle VII sputter coating device for SEM analysis.

3.2.1.2.4 Inductively Coupled Plasma-Mass Spectrometry (ICP-MS)

The components in the synthesized samples were identified using inductivity-coupled plasma (ICP-MS, Perkin Elmer Plasma 400). In order to analyze the samples, about 500 mg of the powdered samples was evaluated by ICP-MS in the Central Lab, METU.

3.2.1.3 Biological Characterization

3.2.1.3.1 Alamar Blue™ Cell Viability Test (Indirect)

A test to determine if pure BAG and Ba-doped BAGs are compatible with cells was conducted in vitro. A human osteosarcoma cell line (Saos-2, ATCC) was employed for experiments involving in vitro cell culture. In DMEM (88%), which has been modified to include 10% (v/v) FBS, 1% penicillin-streptomycin, and 1% sodium pyruvate, Saos-2 bone cells were grown. Cell viability upon indirect contact with substances was assessed using the AlamarBlue™ test (Invitrogen, USA). Cell viability was measured at different incubation periods (1 and 3 days). Four samples

for each group were used for the AlamarBlue^{TM} test. Before cell culture examination, in order to prepare extraction of samples, 1000mg of synthesized BAG and Ba-doped BAG powders were sintered at 200°C for 2h for sterilization. Then, the sterile powders were added to 10 mL complete growth medium and incubated for 24h in the water bath at 37°C. Finally, the extracts were collected with a syringe and poured into sterile falcons using sterile syringe filters to prevent contamination.

Because BAG is basic, the collected extracts from BAG and Ba-doped BAG materials with 0.10 g/mL concentration were diluted with medium starting from 50% in the following order. Extracts were diluted to 0.05 g/mL (X), 0.025 g/mL (X/2), 0.0125 g/mL (X/4), and 0.00625 g/mL (X/8), respectively.

Saos-2 cells were thawed and kept in an incubator containing 5% CO_2 at 37°C for 3 days to achieve 80% confluency, the medium was renewed every day. At the end of 3 days, 10^4 cells were seeded in each well of 96 well-plate and incubated for 24h. After 24h of incubation, and after removal of medium phosphate-buffered saline (PBS) was used to wash cells once, followed by adding 100µL medium to each well. Then 100µL of each extract was added to wells (n=3 and blank=1 (the wells including no cells are called blank)). For control groups, only a complete growth medium with out any extract was used. Finally, the well plate was placed in the incubator for 1 and 3 days.

At the end of each incubation period, extracts were removed, and PBS was used to rinse the cells. Then 100 µL AlamarBlue™ solution (10% v/v), prepared by diluting in DMEM without phenol red, was added to wells. Then the well plate was placed in the incubator in the dark for 4h. After 4h of incubation, the AlamarBlue™ solution of each well was transferred into a new plate, and the microplate reader (μ OuantTM, Biotek Instruments Inc., USA) was used to measure the optical densities of wells at 570 and 600 nm wavelengths.

After recording data, Equation 3.3 was used in order to calculate cell viability.

$$\frac{(O_2 \times A_1) - (O_1 \times A_2)}{(R_1 \times N_2) - (R_2 \times N_1)} \times 100 \quad (3.3)$$

Where:

O_1=molar extinction coefficient (E) of oxidized AlamarBlue (blue) at 570 nm, (80586)

O_2=E of oxidized AlamarBlue at 600 nm, (117216)

R_1=E of reduced AlamarBlue (red) at 570nm, (155677)

R_2=E of reduced AlamarBlue at 600nm, (14652)

A_1=Absorbance of test wells at 570 nm

A_2=Absorbance of test wells at 600nm

N_1=Absorbance of negative control well (media plus AlamarBlue but no cells) at 570nm

N_2=Absorbance of negative control well at 600nm.

After performing the AlamarBlue™ test (Day 1), PBS was used to rinse cells again. Afterward, 100 μL of fresh medium and extracts were added to each well, and the plate was placed into the incubator for 2 more days to perform further AlamarBlue™ tests for day 3. After 3 days, the AlamarBlue™ test was performed, as mentioned on day 1.

3.2.2 Production and Characterization of Barium Doped Baghdadite/PHBV Fibrous Scaffold

3.2.2.1 Production of Barium Doped Baghdadite/PHBV Fibrous Scaffold

A fibrous scaffold of barium-doped BAG/PHBV was produced using the wet electrospinning and freeze-drying method. To produce a fine scaffold using the wet

electrospinning method, a calculated amount (Table 3.2) of BAG and Ba-doped BAG was dispersed in 1,1,1,3,3,3-Hexafluoro-2-propanol (HFIP) and stirred by ultrasonic for 45 minutes to eliminate the risk of agglomeration of nanoparticles (Samani et al., 2019). Then PHBV and PCL with a ratio of 7 to 3 (wt. /wt.) and a total ratio of 14 wt. % was added to the BAG-HFIP and dissolved (Dalgic et al., 2019). Syringe pumps (New Era NE-300, USA), a revolving collector, and a high-voltage power supply (Inovenso, Turkey) were used to set up the electrospinning system. The collector was at a distance of 12 cm from the tip of the nozzle, the syringe pump flow rate was 4 mL/h, and the high voltage was set at 9kV. The scaffold fibbers were collected using an ethanol bath. Each solution was placed in the electrospinning set up for an hour until the nanofibres were spun in the ethanol bath collector. Figure 3.1 shows the schematic illustration of the wet electrospinning system and Figure 3.2 shows the general morphology of the scaffold during and after electrospinning.

Table 3.2 The calculated amount of components used for the preparation of barium-doped baghdadite/PHBV scaffolds

Scaffolds	**HFIP (ml)**	**Pure/Doped BAG (mg)**	**PHBV (mg)**	**PCL (mg)**
1%	4	5.6	392	168
3%	4	16.8	392	168
5%	4	28	392	168

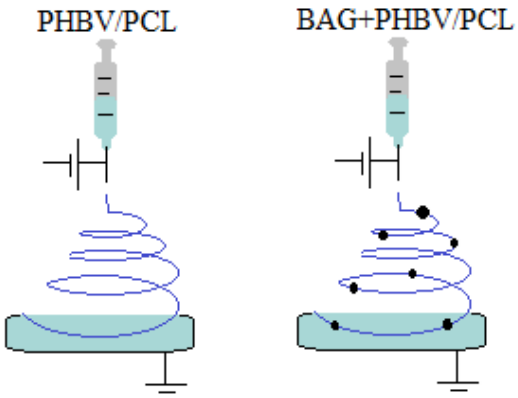

Figure 3.1. Schematic illustration of wet electrospinning system for production of electrospun PHBV/PCL (Left) and BAG bearing PHBV/PCL/BAG fibrous scaffolds.

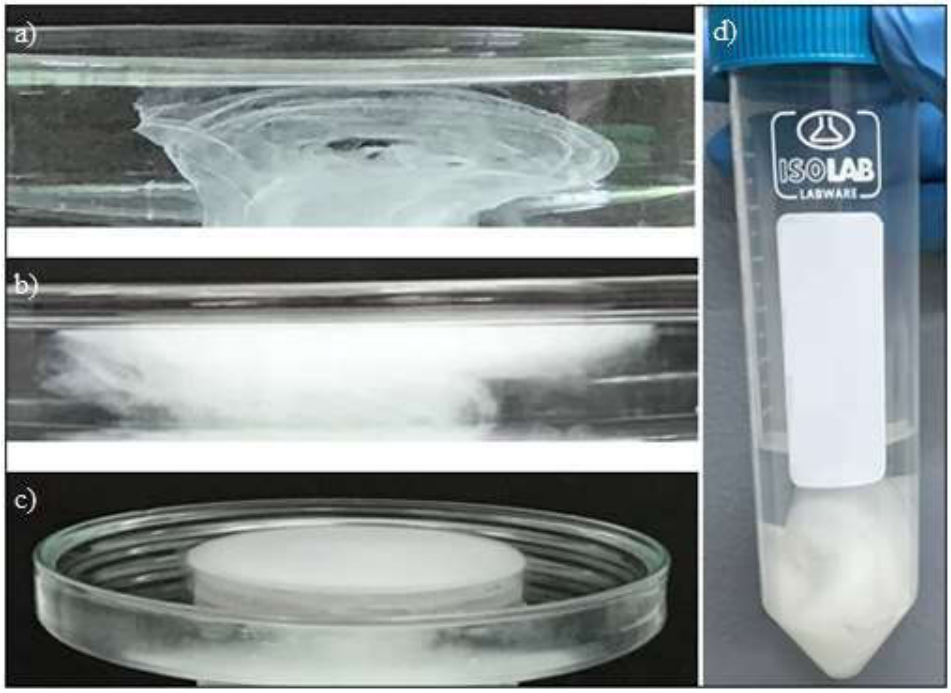

Figure 3.2. PHBV/PCL scaffold formation in an ethanol bath, during (a and b) and after (c and d) electrospinning.

The collected nanofibers were transferred into dH_2O, washed several times, and lyophilized at -80 °C using a freeze dryer for 48 hours after being collected using the electrospinning technique. An image of the scaffold after drying is shown in Figure 3.3.

Figure 3.3. PHBV/PCL wet electrospun scaffold after drying

3.2.2.2 BAG and Ba-Doped BAG+ PHBV/PCL Scaffold Structural Characterization

3.2.2.2.1 Scanning Electron Microscopy (SEM)

The fibrous structure of the BAG+PHBV/PCL and Ba-doped BAG+PHBV/PCL scaffold groups shown in Table 3.2 was examined using SEM analysis. In the Central Lab, METU, SEM analysis was carried out using a QUANTA 400F Field Emission SEM, USA instrument with a resolution of 1.2 nm. With the aid of carbon tape and a Hummle VII sputter coating apparatus, samples were vacuum-coated with gold and mounted onto metal stubs for SEM investigation.

3.2.2.2.2 Determination of Porosity of Scaffolds

To determine the porosity of scaffolds, Archimedes' Principle was applied. In this procedure, samples' dry weight (Wd), a weight suspended in water (Ws), and wet weight (Ww) after being removed from ethanol were all calculated. This experiment used ethanol instead of dH_2O because the samples were floating on water rather than sinking. Three identical segments were punched from each sample. Each sample's weight was determined using a precision scale, and Equation 3.4 was used to get the porosity ratios.

$$Porosity(\%) = \left(\frac{W_w - W_d}{W_w - W_s}\right) \times 100 \quad (3.4)$$

3.2.2.2.3 *In Vitro* Degradation and Water Uptake Test

For the investigation of weight loss and water retention, samples from scaffold groups with comparable sizes and shapes were taken. Samples were weighed before being dipped into PBS (1M, pH 7.4), and they were then incubated for 28 days at 37°C in a water bath that was shaking (Nuve Bath NB 5, Turkey) (PBS was renewed every 2 days). The wet and dry weights of the samples were measured at predefined intervals. Samples were dried in a freeze drier for 10 hours after being rinsed with dH_2O to remove salts. Equations 3.5 and 3.6 were used to compute the weight loss and water retention of scaffolds at various time intervals.

$$weight\ loss(\%) = \left(\frac{M_i - M_f}{M_i}\right) \times 100 \quad (3.5)$$

$$Water\ retention(\%) = \left(\frac{W_w - W_i}{W_i}\right) \times 100 \quad (3.6)$$

Where:

M_i= initial dry weight

M_f= final dry weight

W_w= wet weight

W_i= dry weight.

3.2.2.2.4 *In Vitro* Bioactivity Analysis

Scaffolds were incubated in stimulated body fluid (SBF, pH 7.4), which was made using Kokubo's procedure, to conduct an in vitro bioactivity test (Kokubo and Takadama, 2006). The scaffolds were preserved at 37°C (n=3) for 7 and 14 days after being put within plastic falcons containing SBF. Every two days, SBF solution was replaced, and a pH meter was used to measure the pH of the solution at each time point (S20 SevenEasy TM pH). The scaffolds were immediately rinsed with dH_2O after each incubation time and then dried for 10 hours to remove any remaining moisture. The scaffolds' surface mineralization was examined using SEM analysis, and EDX analysis was used to acquire peaks for the elements Ca and P so that the Ca/P ratios could be calculated.

3.2.2.3 Cell Culture Studies

Human bone osteosarcoma (Saos-2) cells were grown in DMEM supplemented with 10% (v/v) FBS, 1% penicillin-streptomycin, and 1% sodium pyruvate at 37°C in a CO_2 incubator (5% CO_2, 5215 Shel Lab., Cornelius, OR, USA) for cell culture studies. Cells were subcultured when they reached 80% confluency using 0.25% Trypsin/EDTA solution. In this experiment, cells at the 5^{th} passage were used.

To sterilize the scaffolds, they were incubated in 70% ethanol for 2h, and irradiation by UV for 30 minutes on each side was applied. Finally, the scaffolds were incubated in DMEM for 24h before seeding to verify sterilization.

3.2.2.3.1 Alamar BlueTM Cell Viability Test (Direct Contact)

In 96 well plates, Saos-2 cells were seeded at a density of 10^4 cells/scaffold, and they were cultured at 37°C for 7 days in a CO2 incubator. Using the AlamarBlueTM viability assay (n=3), the cell viability of scaffolds was evaluated at various incubation times (days 1, 4, and 7). Every three days, the culture media was refreshed. After each predetermined incubation period, scaffolds were washed with PBS, and AlamarBlue^{TM} solution (10% vol. AlamarBlue^{TM} reagent in DMEM without phenol red) was added. After 4h of incubation, the media in each well was collected, and absorbance measurements at 570 and 600 nm were made with a microplate reader (Module 9200, Turner Biosystem, USA). After removing the AlamarBlue^{TM} solution, scaffolds were washed with PBS, and fresh media were added to continue cultivation. Cell viability was calculated using Equation 3.3.

After day 7, cells were fixed on scaffolds using a 4% formaldehyde solution and prepared for SEM analysis. Briefly, scaffolds were incubated in 4% formaldehyde solution for 20min after washing with PBS. After the incubation period, scaffolds were washed with PBS again and kept in 30, 50, 70, 80, 90, and 100 vol % ethanol, each for 10min. Finally, scaffolds were dried at room temperature.

3.2.2.3.2 Alkaline Phosphate (ALP) Activity Test

To study the osteogenic activity of Saos-2 cells on scaffolds, specific ALP activity (n=3) and intracellular calcium amount (n=3) of cells were measured on days 7 and 14. Different sets of samples were prepared for both days. Scaffolds without cells were used as the negative control. Osteogenic differentiation medium (DMEM containing 10% FBS, 1% penicillin-streptomycin, 1% sodium pyruvate solution, 50 μg/ml ascorbic acid, 10 mM β-glycerophosphate, and 10^{-8} M dexamethasone in ethanol) was used for the incubation of scaffolds for 14 days and 10^4 cells were seeded on each scaffold. In order to obtain cell lysate, cells were freeze-thawed in 300 μl PBS containing 0.1% Triton X-100, and the freeze-thawing process was

repeated 3 times. Lysate (50 µl) and 100 µl PNPP working solution (PNPP substrate solution, Mg-Cl solution, and dH_2O, (10:1:20, vol: vol: vol)) were mixed and incubated on an orbital shaker at 37°C for 60 min. Finally, the absorbance was read at 405 nm with a microplate spectrophotometer (µQuant MQX200, Biotek, USA).

Using different concentrations (0-100 µM) of p-nitrophenol, a calibration curve was constructed and used to determine the amount of p-nitrophenol produced. The ALP activity was normalized by the protein content of cells for each group at the given time point to determine specific ALP activity. The total amount of protein in lysate was measured by the BCA method.

In a summary, bicinchoninic acid solution and Cu_2SO_4 solution (0.04 g of cupric sulfate in 1 ml of water) were combined to create a functional reagent solution (with a ratio of 1 to 50 respectively). Then, for a further hour at 37°C, 25µL of cell lysate and 175µL of BCA solution were incubated on an orbital shaker. Using a microplate spectrophotometer (Quant MQX200, Biotek, USA), the optical density of the samples was measured at 562 nm after incubation. Total protein content was calculated using a calibration curve with known concentrations of bovine serum albumin (BSA) (0-100 µM).

To determine the amount of intracellular calcium, 100 µl of Ca^{2+} stain (containing o-creslophthalein complexone, 8-hydroxyquinoline, hydrochloride acid (1M), and ethanolamine) was mixed with 100 µl of cell lysate and incubated on an orbital shaker at 37°C for 5 min. With the use of a microplate reader (Quant MQX200, Biotek, USA), the absorbance was measured at 570 nm. The calibration curve was produced using various $CaCl_2$ solution concentrations (0-100 µM), and as previously mentioned, the protein content (BCA) of the cell lysate was used to measure and normalize the quantity of intracellular calcium.

3.2.2.4 Mechanical Properties

The uniaxial compressive strength test was used to compare the mechanical properties of several scaffold groups. By freeze-drying the wet electrospun scaffolds in 48 well plates, samples were formed into cylinders. Three samples, each measuring 10 mm in diameter and 8 to 10 mm in height, were created for each scaffold. Using a Univert biomaterial mechanical testing system (Cell scale, Canada) equipped with a 10 N load cell, samples were compressed at a rate of 5 mm/min with a 0.1 N preload and compressed to 65% in strain from their initial size. The plotted stress-strain curves were used to calculate compressive strength and elastic modulus (E).

3.2.2.5 Statistical Analysis

For the statistical analysis of the data, SPSS software (ver. 26.0; IBM Corporation, NY, USA) was employed. A one-way analysis of variance (ANOVA) with the Tukey Post Hoc test was used for multiple comparisons. The outcomes are presented as mean standard deviation (SD).

CHAPTER 4

RESULTS AND DISCUSSION

4.1 Characterization of Synthesized BAG and Ba-Doped BAG Particles

4.1.1 Structural Characterization

4.1.1.1 X-ray Diffraction Analysis (XRD) Results

XRD analysis was performed on four groups of baghdadite samples (BAG, $Ba_{0.075}$-BAG, $Ba_{0.15}$-BAG, and $Ba_{0.3}$-BAG) to identify the presence of phases, calculating lattice parameters and evaluate the effect of Ba doping on these characteristics. The XRD spectra of BAG and Ba-doped BAG samples are presented in Figure 4.1. The characteristic peaks in XRD patterns of all groups were comparable with those of the standard BAG (With JCPDS card 2206-901-96). According to XRD patterns of pure BAG, the sintered samples were not 100% pure and there were a small fraction of other phases, like calcium zirconium oxide ($CaZrO_3$) (JCPDS card 35-0790), and another phase from the Ca-Si family was observed which was found to be "Larnite" (with JCPDS card 4792-901-96). According to the patterns, baghdadite forms the main phase, and Larnite and $CaZrO_3$ are the minor phases (Larnite and $CaZrO_3$ are specified in Figure 4.1). Presence of these phases was observed in other studies (Sadeghzade et al., 2017).

Crystal structure of both BAG and larnite phases was monoclinic. Both phases are made from raw materials (calcium nitrate tetrahydrate, zirconium nitrate oxide, tetraethyl orthosilicate, ethanol, and nitric acid), and the activation energy of both phases was very close to each other. In a study on BAG (Jodati et al., 2022) the same phases were reported while the same temperature (1150°C) was used for sintering.

However, when the XRD patterns of ba-doped samples (Figure 4.1) were analyzed, it was observed that doping barium eliminates the formation of the $CaZrO_3$ phase and reduces the formation of the larnite phase. Thus increasing the Ba amount resulted in a decrease at the larnite phase. According to Figure 4.1, by doping more Ba^{2+} to BAG, peaks get narrower, which means that the crystallinity of samples increases with increasing barium amount. The crystallite size of pure BAG is a close match with the literature (Abbasian et al., 2020).

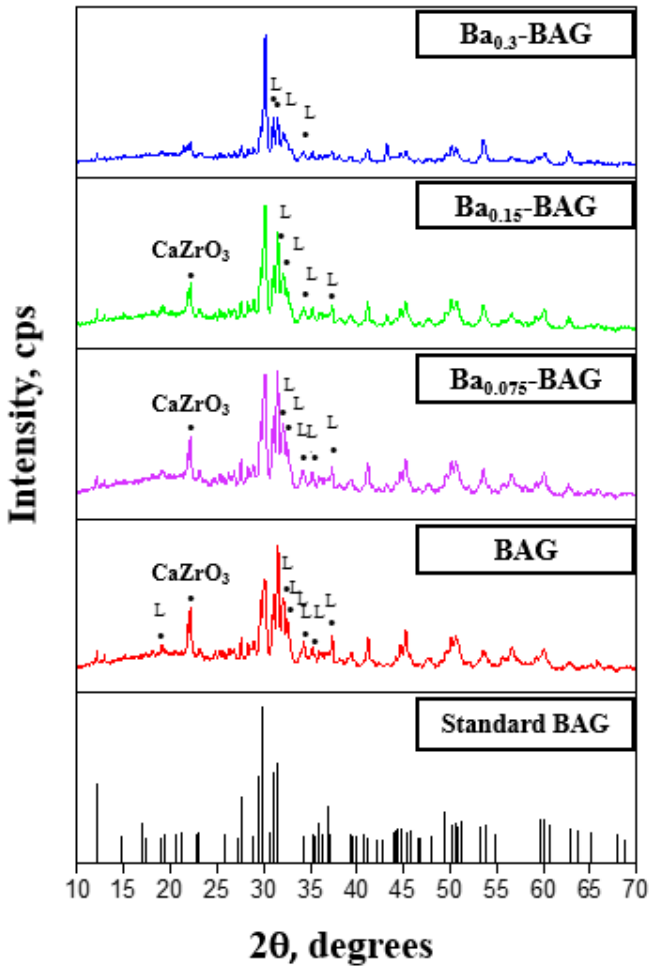

Figure 4.1. X-ray diffraction patterns of standard BAG and prepared samples

The phases calculated by the XRD patterns of BAG and Ba-doped BAG groups and by using Highscore software are presented in Table 4.1. Accordingly, even a small amount of Ba doping causes a decrease in larnite percentage.

Table 4.1 Amount of BAG and Larnite phases in samples

Sample	**BAG (%)**	**Larnite (%)**	**$CaZrO_3$ (%)**
Pure BAG	86	13	1
$Ba_{0.075}$-BAG	86.86	12.19	0.95
$Ba_{0.15}$-BAG	87.15	12.15	0.70
$Ba_{0.3}$-BAG	87.72	12.28	0

The Crystallinity degree of the samples is presented in Table 4.2. According to this table, the highest degree of crystallinity belongs to the sample with the highest amount of doped barium.

XRD patterns of pure and doped BAGs exhibited well-defined peaks. However, a shift to the lower 2θ values was observed when Ba-doped BAG groups are compared to the pure BAG group. This can be because of the difference between the ionic ratio of Ba^{2+} and Ca^{2+}. It has been indicated by other researchers that doping an element with greater ionic size like Sr^{2+} with hydroxyapatite (HA) (Sr^{2+} replaced with Ca^{2+} in HA structure) can cause a shift of peaks to the lower 2θ values (Yedekçi et al., 2022). Hence, since Ba^{2+} has a greater radius (1.35Å) than Ca^{2+} (0.99Å), the movement of peaks to the lower values of 2θ is reasonable, and it can cause an increase in the lattice parameters as expected from the literature. In a study on Ba-doped HA, the same behavior towards change to the lower values of 2θ was observed. Doping Ba caused an increase in the unit cell dimensions, and therefore, these results also indicated that the doping process was successful (Senthilkumar et al., 2021). Calculated lattice parameters for prepared samples in this study are provided in Table 4.2.

Table 4.2 The average crystallite size, lattice parameters, and average crystallinity degree of BAG and Ba-doped BAG groups

Groups	Crystallite Size (nm)	Lattice parameters					Crystallinity Degree (%)
		a (Å)	b (Å)	c(Å)	Volume(Å^3)	β(°)	
BAG	29.07	7.29	10.06	10.58	776.77±0.1	90.68	95.52
$Ba_{0.075}$-BAG	29.58	7.29	10.06	10.60	778.91±0.1	90.68	96.75
$Ba_{0.15}$-BAG	29.75	7.30	10.07	10.56	778.21±0.1	90.70	96.78
$Ba_{0.3}$-BAG	30.32	7.31	10.09	10.57	781.11±0.1	90.75	96.81

The observed peaks of powder complied with the peaks of standard synthetic BAG with JCPDS card 2206-901-96, which has unit cell parameters of a=7.36 Å, b=10.17 Å, c=10.45 Å, β=90.87°, and volume=782.72 Å^3 with space group $P2_1/c$ that describes the symmetry of the crystal. It is worth mentioning that the surface morphology of BAG powders synthesized using the sol-gel method depends on solution properties, sol-gel parameters, and heating regimes.

4.1.1.2 Fourier Transform Infrared Spectroscopy (FTIR) Results

FTIR spectra of BAG and Ba-doped BAG groups were analyzed to determine BAG-related specific absorption bands and changes in these bands due to chemical interactions with doped Ba. FTIR spectroscopy reveals the presence of functional groups related to BAG (Figure 4.2). As shown in the FTIR pattern of baghdadite, an absorption band corresponding to the isolated group of SiO_4 is observed in the wavenumber range of 800 to 1000 cm^{-1}. According to Figure 4.2, the absorption band in the range of 600-750 cm^{-1} is related to the Si-O-Si vibration. Moreover, the observed absorption band in the range of 450-600 cm^{-1} can be ascribed to the Ca-O bond. Finally, the absorption at 996 cm^{-1} is assigned to the Si-O-Zr vibration. All the

bonds mentioned above were observed in all samples and they are presented in Table 4.3. In a study on baghdadite-vancomycin scaffolds (Bakhsheshi-Rad et al., 2017) it has been indicated that baghdadite includes an absorption band in the range of 800-1000 cm^{-1} which attribute to the isolated group of SiO_4 and in the range of 600-750 cm^{-1}, was belong to Si-O-Si vibration. In the same study, the presence of a band with a smaller wavenumber between 450 to 600 cm^{-1} was mentioned which is an attribute of the CaO bond. Moreover, there are adsorption bands attributed to the Si–O–Zr vibration between 900-1050 cm^{-1}. The wavenumbers presented in the mentioned study are closely matched with the results of this thesis.

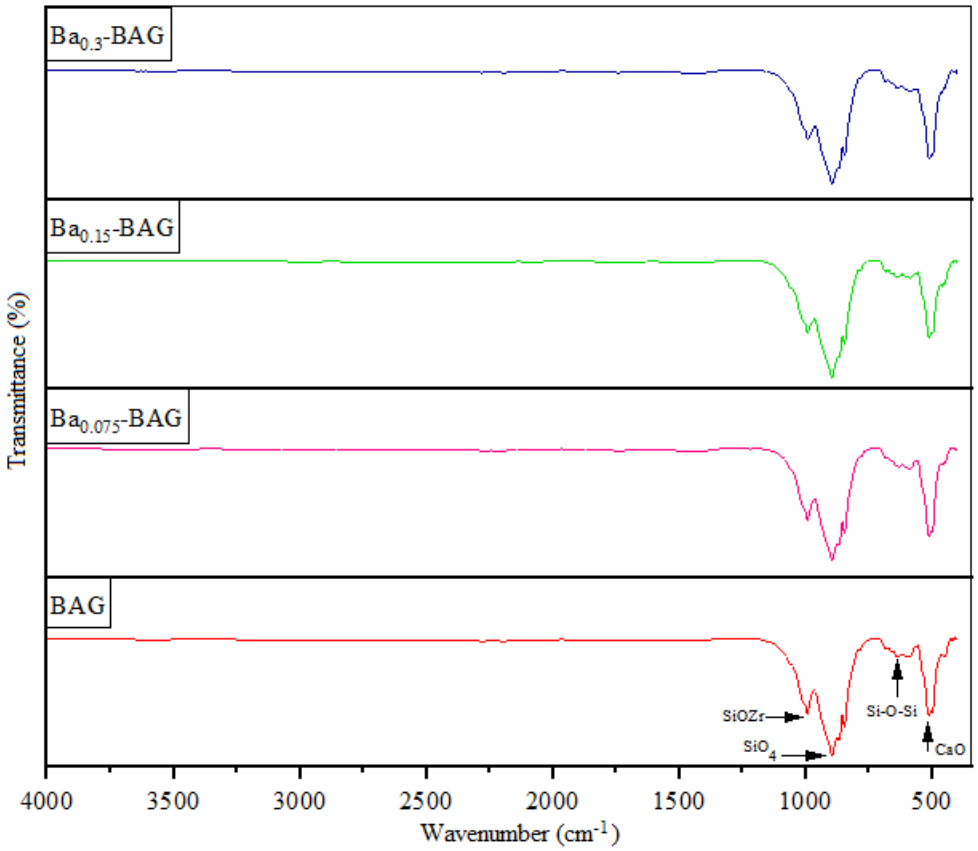

Figure 4.2. FTIR spectra of the BAG and Ba^{2+} doped BAG samples

Table 4.3 Assignments of FTIR absorption bands to chemical groups of prepared samples.

Functional Groups	Wavenumber (cm^{-1})			
	BAG	**$Ba_{0.075}$-BAG**	**$Ba_{0.15}$-BAG**	**$Ba_{0.3}$-BAG**
SiOZr	996	996	994	994
SiO_4	901	899	898	898
Si-O-Si	664	644	644	644
Cao	517	515	513	513

In another study on Zn-doped BAG (Yadav et al., 2021), similar bands were observed, with the ones obtained in spectra of doped BAG here. Doping Ba with BAG has not created a new band, and it has only caused a slight change of absorption bands to the lower values as given in Table 4.3. Likewise, in the study on doping Zn to BAG (Yadav et al., 2021), no additional new bands were reported. In another study by (Mugundan et al., 2022), it has been indicated that, when the Ba-doped amount is very low, no effect on present absorption bands or additional bands was observed. Finally, in a study on Ba-doped polyvinylchloride (PVC) (Gholamzadeh et al., 2022) it has been reported that once Ba was introduced to the structure, only a slight shift to the lower wavenumber happened. All the above-mentioned reports support the findings in this thesis. Here as the doping amounts of Ba were also small (up to 0.3 M) it was considered to have similar results in the literature about FTIR analysis results of doping BAG with other elements.

4.1.1.3 Scanning Electron Microscopy (SEM) Analyses of the BAG and Ba-Doped BAG

Synthesized BAG and Ba-doped BAG particles were analyzed by SEM for investigating their general shapes and particle morphologies. As shown in Figure 4.3, the BAG particles were more distinct and slightly smaller than the Ba-doped BAG ones.

Their average grain sizes measured from SEM images, using ImageJ software are presented in Table 4.4. As observed in Figure 4.3 and Table 4.4, the particle size of BAG is growing up by increasing the Ba doping.

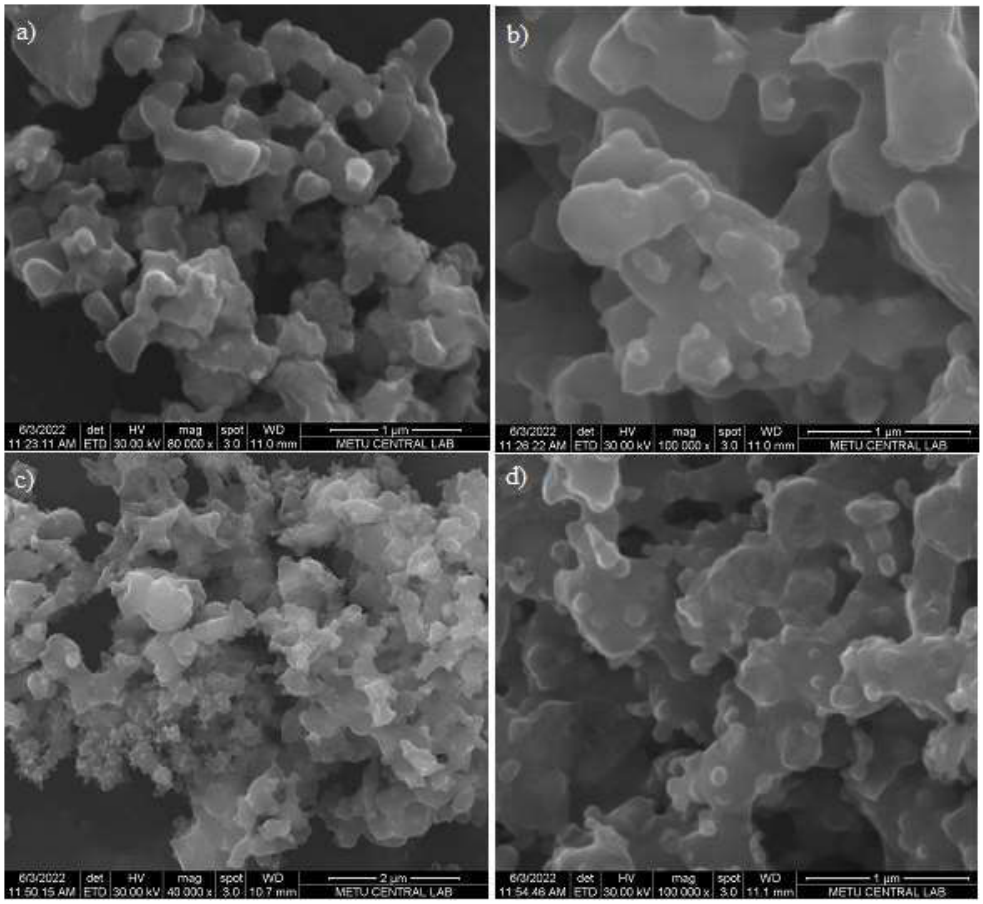

Figure 4.3. SEM images of prepared samples; a) BAG, b) $Ba_{0.075}$-BAG, c) $Ba_{0.15}$-BAG, d) $Ba_{0.3}$-BAG

By evaluating the SEM images of Ba-doped BAG, it is observable that doping Ba ions affect the morphology of BAG. The grain size of particles in samples including Ba is larger than pure BAG increasing in proportion with the increase in Ba amount (Table 4.4). It is worth mentioning that the irregularity of grains and agglomeration is also growing by increasing the Ba amount. Particles have irregular, spherical, and tightly packed agglomerated structures. The large agglomerates have been formed

due to the presence of surface energy as well as the desire of BAG particles to stick together (Arefpour et al., 2019).

Table 4.4 The average grain size of samples with different Ba amounts

Samples	Average Grain Size (nm)
BAG	124.05±8.21
Ba0.075-BAG	124.58±8.21
Ba0.15-BAG	125.18±6.10
Ba0.3-BAG	135.38±11.64

In a study on BAG by (Jodati et al., 2022) it has been indicated that grains are formed as the result of the agglomeration of crystals, and sometimes the small grains match the crystallite size (which are presented in Table 4.2), but grains are often constructed due to the combination of several crystallites and are therefore larger than them.

4.1.1.4 Inductively Coupled Plasma-Mass Spectrometry (ICP-MS)

Chemical composition is an effective parameter that plays an important role in cell behavior (Arefpour et al., 2020). Therefore it is important to verify the chemical composition of doped BAG groups according to doping amounts. The chemical composition of Ba-doped BAG powders was obtained from ICP-MS analysis (Table 4.5). This analysis confirms the presence of Ba in the powders, which indicates that doping Ba ions into the BAG structure was successful. The similarity in theoretical and measured Ba ratios was also recognizable and supportive for successive doping in the proposed amounts. According to the literature, the molar ratio of Ca: Zr: Si in the BAG structure is equal to 3:1:2, respectively (Jodati et al., 2020). Considering the results of the ICP analysis, this ratio is approximately maintained. For samples with Ba in their structure, a decrease in the Ca amount is notable as the Ba amount increases, which can be due to the replacement of Ca with Ba ions in the doping

process (as expected). The ICP results indicated that the Ca:Zr:Si: Ba molar ratio between all groups is within an acceptable range.

Table 4.5 Chemical composition of BAG and Ba doped BAG groups as measured by ICP

Sample	**Theoretical Molar Ratios**				**Measured Molar Ratios by ICP**			
	Ca	**Zr**	**Si**	**Ba**	**Ca**	**Zr**	**Si**	**Ba**
BAG	3	1	2	-	3±0.1	0.81±0.01	1.99±0.01	-
$Ba_{0.075}$-BAG	2.925	1	2	0.075	2.9±0.1	0.77±0.02	2 ±0.01	0.07±0.01
$Ba_{0.15}$-BAG	2.85	1	2	0.15	2.86±0.1	0.77±0.02	1.97±0.01	0.144±0.01
$Ba_{0.3}$-BAG	2.7	1	2	0.3	2.75±0.1	0.75±0.02	1.87±0.01	0.3±0.01

It is noticeable from the table that the experimental ratios of Ca match the theoretical values, however, Si and Zr measured values are slightly smaller than theoretical values. This difference could be due to the formation of the larnite phase. It has been indicated by (Jodati et al., 2022) that Si quickly reacts with Ca, even before the presence of Zr, and it creates the Ca-Si phases. It has been reported in another study (Evis, 2007), that in the presence of zirconia, calcium oxide can form $CaZrO_3$, in a result, a small amount of Zr ion could not be located in the BAG structure and instead, it reacts with Ca and forms $CaZrO_3$ phase.

4.1.2 Biological Characterization

4.1.2.1 Cell Viability Tests of BAG and Ba-Doped BAG Particles (Indirect Assay)

The viability of Saos-2 cells treated with BAG and Ba-BAG particle extracts was studied to evaluate the cytotoxicity of the synthesized particles on osteoblast cells. The collected extracts from BAG and Ba-BAG materials were diluted to 0.05 g/mL (X), 0.025 g/mL (X/2), 0.0125 g/mL (X/4), and 0.00625 g/mL (X/8) concentrations with cell culture media. Cells grown in a complete growth medium were used as the positive control group. On the first day, the relative cell viability of all samples was lower than the positive control group, but only the samples with the highest concentration (0.05 g/mL) were slightly toxic, and the rest of the concentrations showed no toxic effects (Figure 4.4). On the first day, the cell viability of Ba-BAG samples was slightly lower than pure BAG, but at the lowest dilution and highest Ba-doped amount, cell viability was increased and passed the pure BAG. But these differences are not statistically significant.

On the third day of incubation, all the samples having a concentration of 0.05 g/mL showed a toxic effect similar to the first day. Also, pure BAG showed a toxic effect on the concentration of 0.025 g/mL and 0.0125 g/mL, which could indicate that BAG extracts do not positively affect cell viability at these concentrations. On the other hand, the cell viability of the Ba-doped BAG samples increased significantly on the third day. Comparing the three concentrations of Ba-BAG (X/2, X/4, and X/8) on the third day could illustrate the positive effects of doping a specific amount of Ba^{2+} with BAG. Statistical analysis showed no significant differences between Ba-doped BAG samples in X/4 and X/8 concentrations. Based on the AlamarBlue™ assay of pure BAG and Ba-doped BAG samples on day 1 and day 3, compared with positive control groups, we can assume that cell viability in Ba-doped BAG extracts increased with an increasing incubation period.

In a study on BAG (Jodati et al., 2022), it has been indicated that BAG has no cytotoxic effects on Saos-2 cells, however, after 48h of incubation, a slight decrease in the viability even in control groups was observed, was due to reaching the 80% confluency. According to Figure 4.4, and by comparing days 1 and 3, a slight decrease in some of the groups is noticeable, which can be the result of reaching confluency as mentioned in the literature.

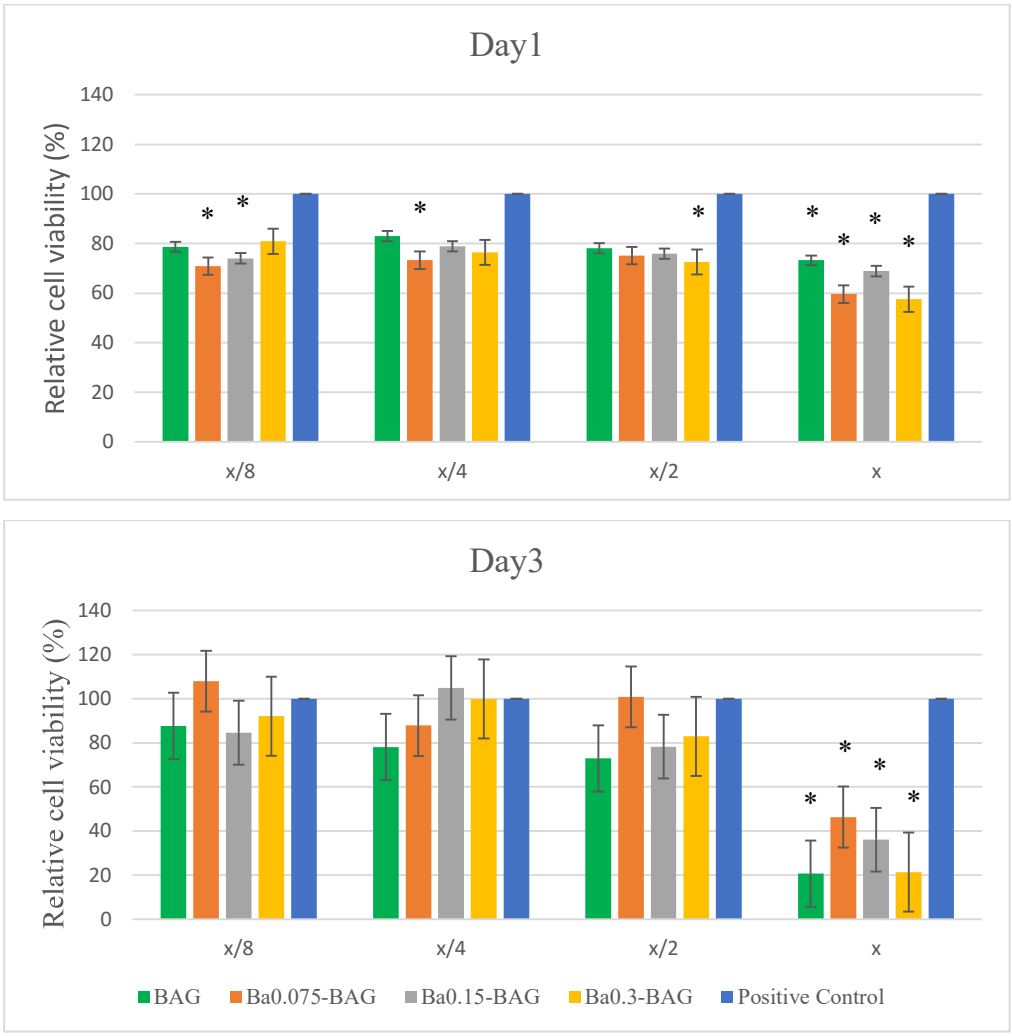

Figure 4.4. Relative viability of Saos-2 cells on pure and doped BAG on days 1 and 3. The error bars represent the standard error of means. * indicates a statistically significant difference (<0.05) between groups and positive control.

Cell viability assay results showed that the Ba^{2+} doped BAG was non-toxic and could promote cell proliferation at specific amounts. In this thesis, the AlamarBlue™ assay indicated that doping Ba^{2+} with BAG has positive effects on cell viability.

4.2 Characterization of BAG+PHBV/PCL and Ba-doped BAG+PHBV/PCL 3D Electrospun Scaffolds

4.2.1 Structural Characterizations

4.2.1.1 Scanning Electron Microscopy (SEM) Analysis of the Scaffolds

SEM analysis was used to observe the fibrous structure and morphological properties of electrospun scaffolds groups. The diameter of the fibers was studied using SEM results and ImageJ software. SEM images of the scaffold groups showing the distribution and shape of fibers and the average diameters of the fibers in each group are presented in Figure 4.5. In this study, average diameter of electrospun PHBV/PCL fibers is 1.87 μm, which is a close value to those in the literature (Dalgic et al., 2019). Adding particles into fibers during electrospinning generally causes a decrease in the average diameter. The average diameter of samples with 1%, 3%, and 5% BAG and Ba-doped BAG, varies between 1.87-1.22 μm. As the BAG amount increases the diameter of fibers decreases and this decrease more with the increasing amount of Ba (Presented in Figure 4.5).

In a study on electrospun PHBV/PCL/incorporated with Diatome silica frustules (DS) (Dalgic et al., 2019), it has been indicated that the average diameter of PHBV/PCL fibers is 1.38±0.2 μm and incorporating DS particles results in a thicker fiber formation. Moreover, the addition of DS resulted in the presence of both nano and microfibers, which were reported to promote cell proliferation and ALP activity of Saos-2 cells, and better mimic the bone extracellular matrix.

The effect of BAG on electrospun PCL/graphene scaffolds was studied in another study (Samani et al., 2019) and it has been indicated that BAG causes a decrease in the diameter of fibers, which supports the finding in this thesis.

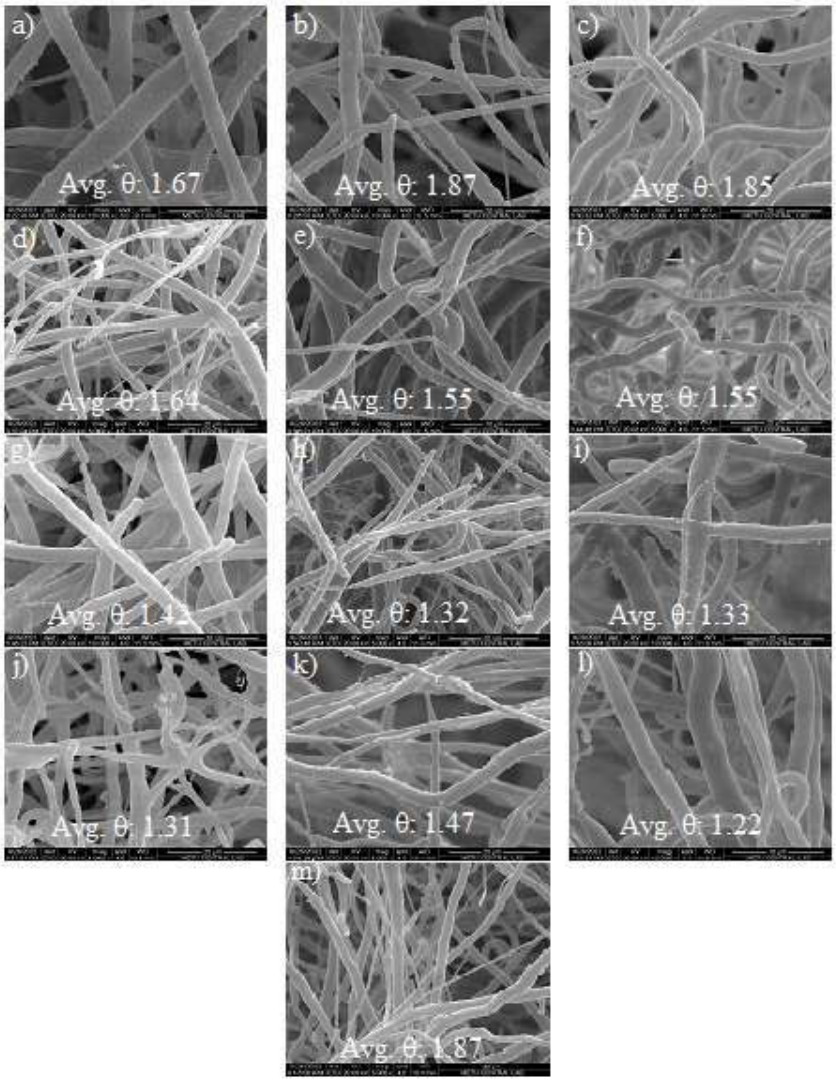

Figure 4.5. SEM images of scaffolds. a) BAG1%+PHBV/PCL, b) $Ba_{0.075}$-BAG1%+ PHBV/PCL, c) $Ba_{0.15}$-BAG1%+ PHBV/PCL, d) $Ba_{0.3}$-BAG1%+ PHBV/PCL, e) BAG3%+ PHBV/PCL, f) $Ba_{0.075}$-BAG3%+ PHBV/PCL, g) $Ba_{0.15}$-BAG3%+ PHBV/PCL, h) $Ba_{0.3}$-BAG3%+ PHBV/PCL, i) BAG5%+ PHBV/PCL, j) $Ba_{0.075}$-BAG5%+ PHBV/PCL, k) $Ba_{0.15}$-BAG5%+ PHBV/PCL, l) $Ba_{0.3}$-BAG5%+ PHBV/PCL, m) PHBV/PCL.

4.2.1.2 Determination of Porosity of Scaffolds

The porosity and density of scaffolds were analyzed and the results are presented in Table 4.6. According to porosity measurements, the porosity of the PHBV/PCL scaffold group had the highest value; 78%. This percentage decreases about 1-2% (around 76-77%) when there is BAG in the scaffold's structure. It was observed that by increasing the Ba^{2+} amount, the porosity of the same BAG content groups showed slightly decreased porosity (72-76%).

In the study on the electrospun PHBV/PCL/DS scaffolds (Dalgic et al., 2019) porosity of PHBV/PCL was reported to be about 76% and it decreases as the DS is introduced to the structure. In this thesis, the porosity also decreased with the BAG and Ba-doped BAG addition. The slight difference between the porosity of electrospun PHBV/PCL scaffolds could be because of the difference between spinning rate, voltage, and distance-like parameters (Samani et al., 2019). It has been reported in the literature (Tavangar et al., 2020) that doping Ba decreases the porosity of HA scaffolds due to the bigger grain size of Ba-doped HA compared with HA scaffolds (Because Ba fills the pores of HA scaffolds. In this thesis, Ba has the same effect on the porosity of samples. In the process of doping, Ba is taking the place of Ca in the BAG structure, and due to Ba's higher radius, the pores are filled resulting in a decrease in the porosity of scaffolds containing Ba. Incorporating BAG covers more space between fibers thus resulting in the reduction of porosity, and doping Ba covers even more space and reduces the porosity of scaffolds.

Table 4.6 Porosity of electrospun scaffolds

Sample	Porosity (%)
BAG1%+PHBV/PCL	77.58±1.71
$Ba_{0.075}$-BAG1%+PHBV/PCL	76.05±2.17
$Ba_{0.15}$-BAG1%+PHBV/PCL	75.69±2.40
$Ba_{0.3}$-BAG1%+PHBV/PCL	74.25±3.27
BAG3%+PHBV/PCL	76.62±3.71
$Ba_{0.075}$-BAG3%+PHBV/PCL	75.27±0.84
$Ba_{0.15}$-BAG3%+PHBV+PCL	74.71±4.41
$Ba_{0.3}$-BAG3%+PHBV/PCL	73.23±3.89
BAG5%+PHBV/PCL	76.22±4.19
$Ba_{0.075}$-BAG5%+PHBV/PCL	74.90±4.00
$Ba_{0.15}$-BAG5%+PHBV+PCL	73.76±2.19
$Ba_{0.3}$-BAG5%+PHBV/PCL	72.87±1.56
PHVB/PCL	78.78±1.71

Statistically controlling the porosity showed no significant difference between groups.

4.2.1.3 *In Vitro* Degradation and Water Uptake Test Results of Scaffolds

The in vitro degradation and water uptake were performed to determine the weight loss of prepared samples (n=3) over 28 days of incubation in the PBS and the results are presented in Figure 4.6. In the first week of incubation, the degradation was up

to 5-6 %, but after the fourth week, the degradation increased to 19-20 %. Based on the results, the degradation rate of the electrospun PHBV/PCL was around 2 % after 7 days of incubation, and this rate increased when pure BAG was introduced to the structure. However, presented in Figure 4.6, the degradation rate decreases when Ba is introduced to BAG.

It has been reported (Dalgic et al., 2019) that PHBV is a hydrophobic polymer with a very low degradation rate and the measured degradation rate of these electrospun polymers was reported to be around 2.8-3 % during 7 days of incubation in PBS. Additionally in the same study (Dalgic et al., 2019) the water uptake of the scaffolds was reported to be in the range of 200-900% during 7-28 days of incubation. The water uptake of the samples should be at the controllable level because the high amount of water uptake means the swelling of the scaffolds and increases the dislocation risk for an implanted scaffold.

In the study on BAG (Jodati et al., 2022), the degradation rate of discs with pure BAG was evaluated, and it was reported that BAG has a high degradation ability. In another study (Sadeghzade et al., 2020) calculated the weight loss of composite scaffolds of BAG/diopside (85/15 wt. %) from 3.5 to 15.1% after 7 to 28 days of incubation in PBS at 37°C and they showed that 51% weight loss was observed in pure BAG scaffolds after 28 days of immersion in PBS. Likewise, (Abbasian et al., 2020) measured the weight loss of BAG/nylon 6 scaffolds in PBS buffer solution as a function of soaking time. This work showed that the weight loss of pure polymeric scaffolds was only 4.5% after 28 days of immersion, but the weight loss of composite scaffolds with only 10 wt. % BAG reached 15.4% at the end of 28 days. Based on these studies, to modify the high degradability of BAG scaffolds, a polymer, in this case, poly (caprolactone fumarate), was used as a coating material, which resulted in a decrease in the degradation rate to nearly 91% after 7 days of immersion. Likewise, using PCL/ bioactive glass as coating decrease the weight loss of BAG scaffolds from 10% to almost 4% after 28 days of immersion (Roohani-Esfahani et al., 2012). The mentioned findings can support the greater degradation rate of groups including BAG when compared with pure polymer. Finally, it has been reported that Ba has a

low degradation rate, so by doping Ba to BAG the high degradation rate of BAG is controllable, as is observed in the results.

No statistically significant differences were observed between scaffold groups.

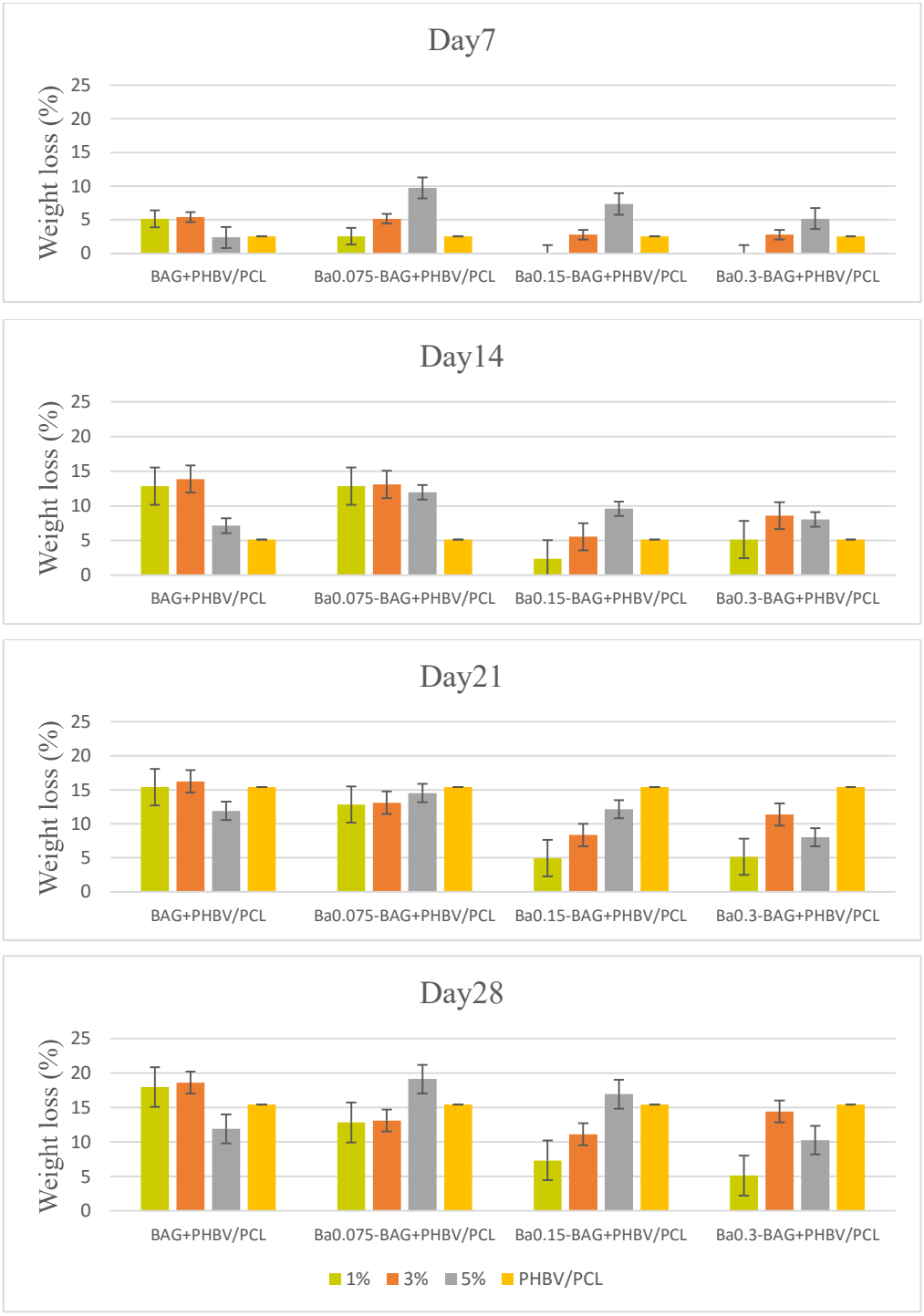

Figure 4.6. Total weight loss of scaffold groups after different PBS (0.01 M, PH: 7.4, at 37 °C) incubation periods.

As plotted in Figure 4.7, the water uptake of the prepared samples was about 200-250 wt% in the first week, and then on the third week of incubation, it reached the peak amount (350-450 wt%), and finally on the fourth week in decreases to 180-250 wt%. Thus water uptake results were compatible with the above requirements defined in the literature (Dalgic et al., 2019).

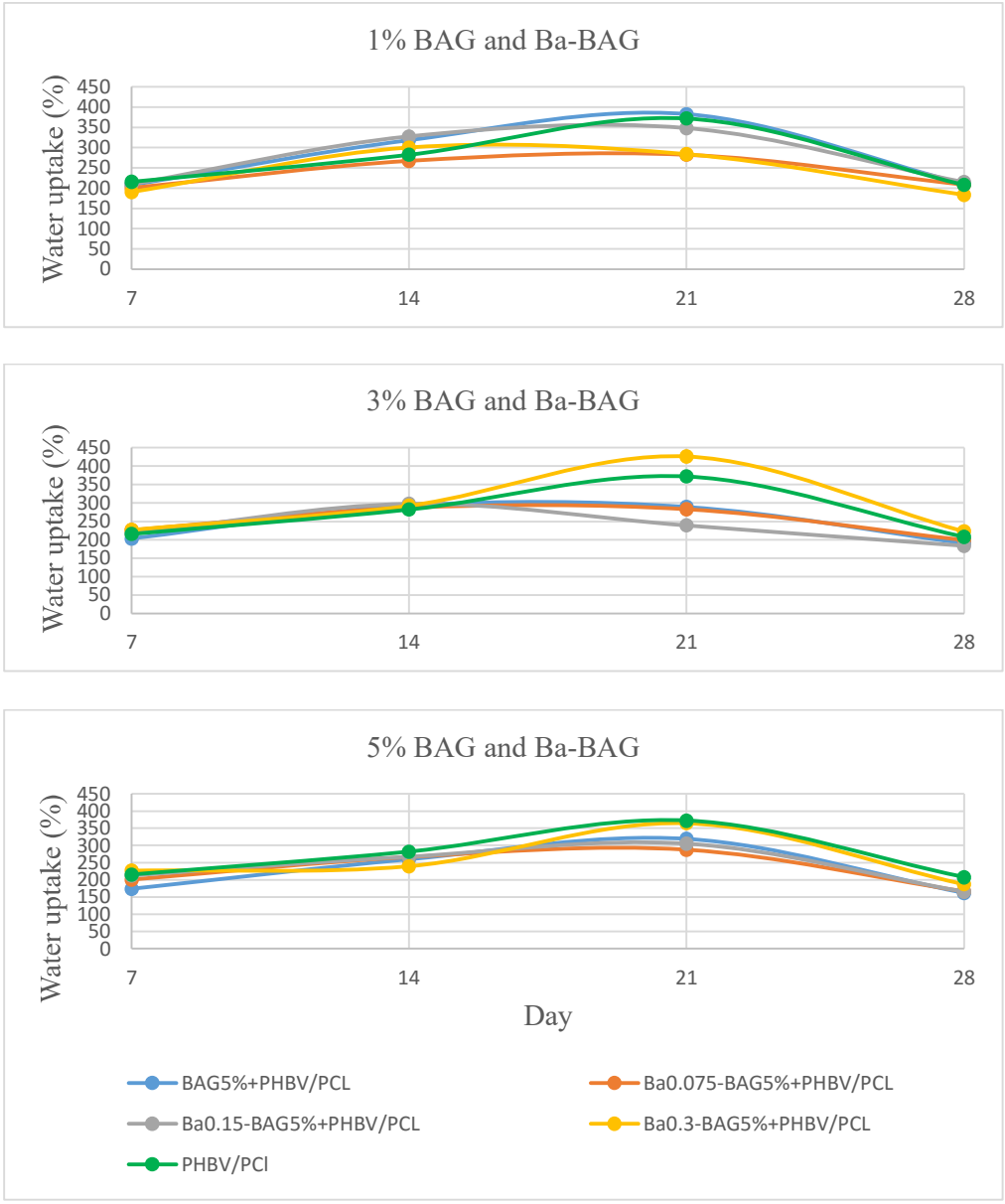

Figure 4.7. Water uptake of the scaffold groups over 28 days of incubation in PBS.

4.2.1.4 *In vitro* Bioactivity Test Results

The bioactivity of the scaffolds was determined by placing scaffolds (n=3) in SBF solution for different incubation periods (days 7 and 14). In vitro bioactivity test survey as a tool to predict the bonding of host tissue with scaffolds through CaP involving mineral formation during in vivo conditions (Kokubo and Takadama, 2006). Kokubo proposed the use of FBS because of the similarity of ionic concentration to the inorganic parts of human blood plasma. They have also reported that the Ca/P ratio of the formed apatite crystals on the surface of ceramics and composites is 1.67, which is the stoichiometric ratio of these elements in hydroxyapatite.

Samples were examined with SEM and EDX analysis before soaking into the SBF and no apatite-like mineral was detected in the chemical composition of the surfaces. After 7 days, CaP mineralization (the main component of apatite) occurred on all scaffolds incubated in SBF solution (Figure 4.8). On day 7, the apatite particles were in agglomerated form and smooth, and on day 14, they covered the fibers extensively. This change in the morphology of the apatite formation is assigned to the crystallinity degree of formed apatites (Siriphannon et al., 2002). In the study on BAG, (Jodati et al., 2022) similar observation was reported after 14 days of incubation in SBF, which was concluded as the ability of BAG to promote bioactivity.

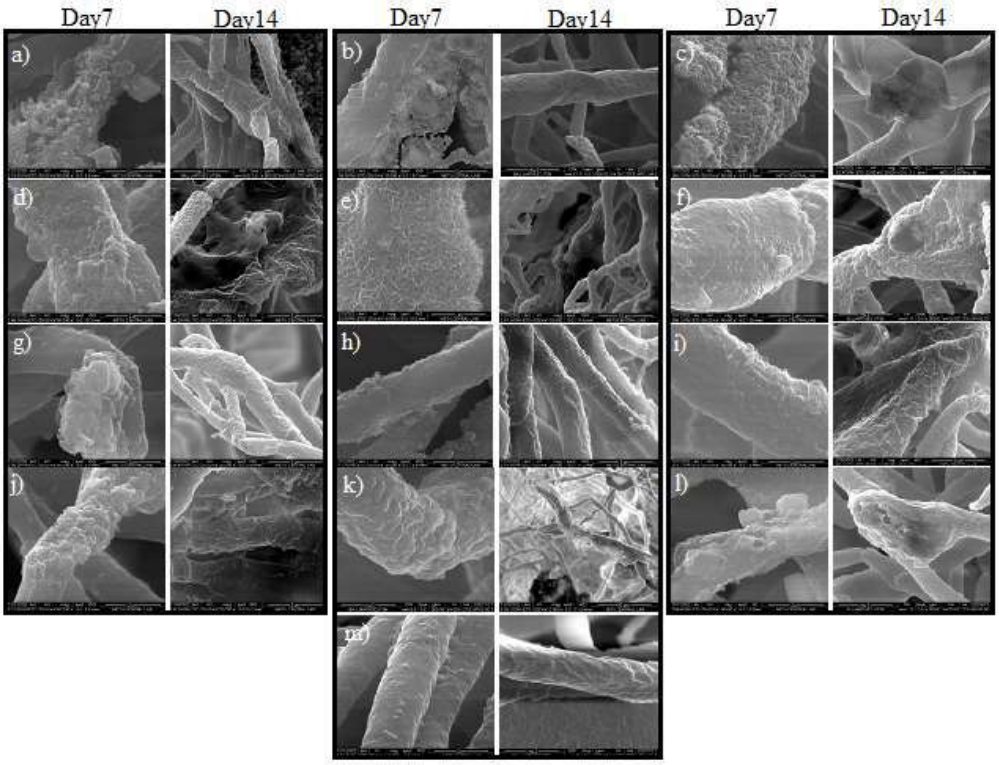

Figure 4.8. SEM image of scaffolds after soaking in FBS for 7 and 14 days: a) BAG1%+PHBV/PCL, b) $Ba_{0.075}$-BAG1%+ PHBV/PCL, c) $Ba_{0.15}$-BAG1%+ PHBV/PCL, d) $Ba_{0.3}$-BAG1%+ PHBV/PCL, e) BAG3%+ PHBV/PCL, f) $Ba_{0.075}$-BAG3%+ PHBV/PCL, g) $Ba_{0.15}$-BAG3%+ PHBV/PCL, h) $Ba_{0.3}$-BAG3%+ PHBV/PCL, i) BAG5%+ PHBV/PCL, j) $Ba_{0.075}$-BAG5%+ PHBV/PCL, k) $Ba_{0.15}$-BAG5%+ PHBV/PCL, l) $Ba_{0.3}$-BAG5%+ PHBV/PCL, m) PHBV/PCL.

In another study on BAG (Schumacher et al., 2014), the ability of BAG to promote bioactivity after 7 days of incubation in SBF was also reported. According to another study doping Ba with bioactive glass in low concentrations promoted bioactivity (Arepalli et al., 2015), which suggests that barium can enhance bioactivity. Accumulations of minerals for such apatite-like structures on the surface of PHBV/PCL scaffolds were considerably less suggesting the improvement of bioactivity even with a 1 % BAG addition. It can be suggested that as BAG content increased the apatite formations were also improved as there were denser (thick) coatings on the fibers for larger BAG % groups (3 and 5%). The results of the EDX analysis are presented in Table 4.7.

Table 4.7 Ca/P ratio of scaffold groups calculated from EDX analysis.

Samples	Ca/P	
	Day7	**Day14**
BAG1%+PHBV/PCL	3.27	0.4
$Ba_{0.075}$-BAG1%+PHBV/PCL	1.44	2.56
$Ba_{0.15}$-BAG1%+PHBV/PCL	2.38	3.75
$Ba_{0.3}$-BAG1%+PHBV/PCL	1.4	3.09
BAG3%+PHBV/PCL	1.73	2.96
$Ba_{0.075}$-BAG3%+PHBV/PCL	2	2.75
$Ba_{0.15}$-BAG3%+PHBV/PCL	2.02	1.35
$Ba_{0.3}$-BAG3%+PHBV/PCL	1.53	1.57
BAG5%+PHBV/PCL	1.14	1.65
$Ba_{0.075}$-BAG5%+PHBV/PCL	1.56	6.16
$Ba_{0.15}$-BAG5%+PHBV/PCL	1.85	0.78
$Ba_{0.3}$-BAG5%+PHBV/PCL	5	0.26
PHBV/PCL	0.66	0.75

Finally, the pH changes of the SBF during incubation periods were measured and plotted (Figure 4.9). The pH of the solutions increased in the first week to approximately 7.7 and reached its maximum value and then it started to decrease to about 7.4 on day 14 of incubation.

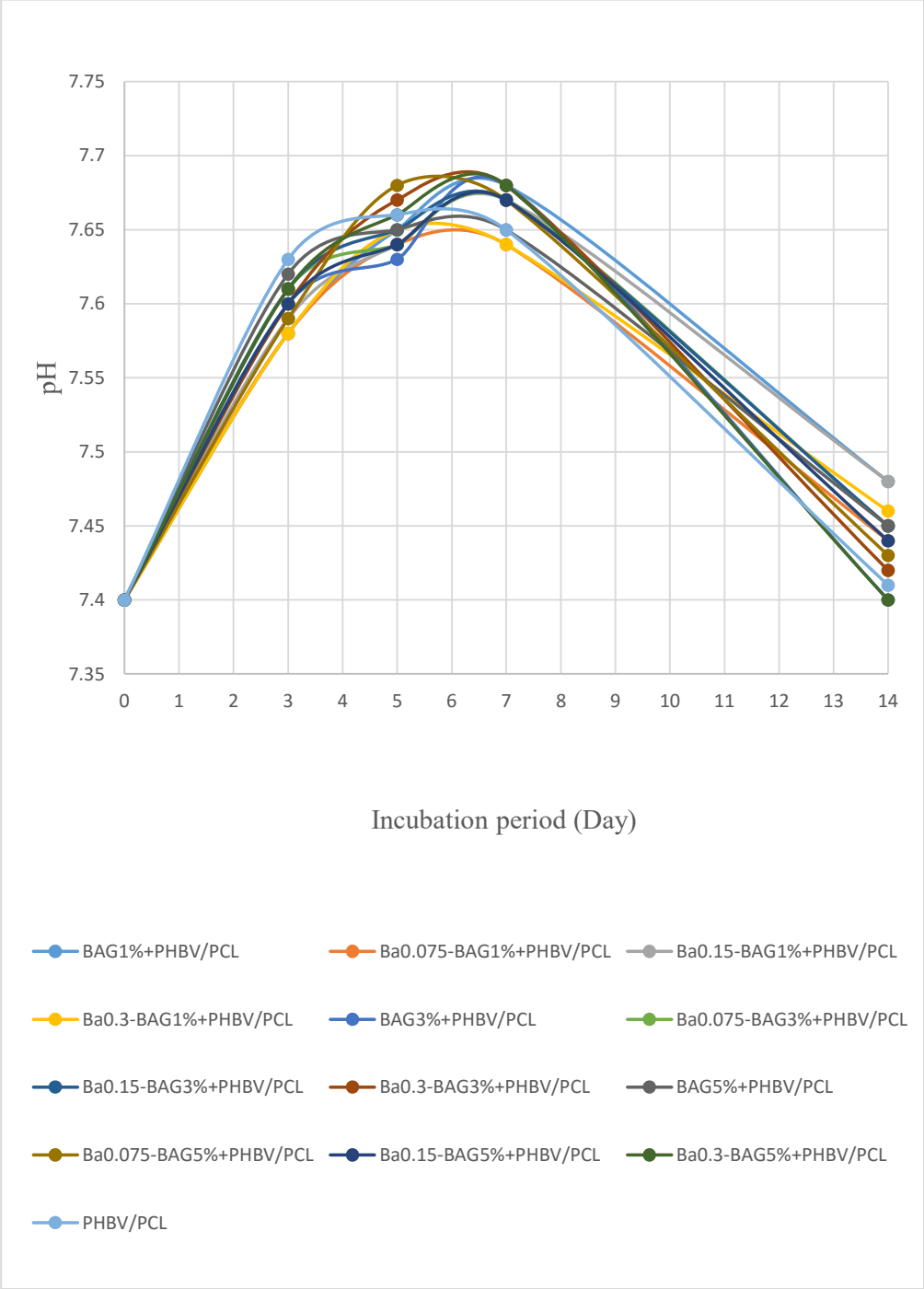

Figure 4.9. Change in the pH of SBF in which PHBV/PCL, BAG, and Ba doped BAG scaffolds were incubated (n=3)

4.2.2 Biological Characterization

4.2.2.1 Cell Viability and Proliferation on Scaffolds

The viability of Saos-2 cells on scaffolds was examined with direct contact tests to evaluate scaffolds' potency for attachment and Support of proliferation of bone cells. Pure PHBV/PCL scaffolds were used as a control group.

Approximately all the groups showed good cell viability when compared with only polymer scaffolds that are known to be biocompatible in literature. In all groups increase in viabilities as an indication of proliferation was very slow from day 1 through day 7 (for ex. From 16 % to 28 % in BAG5%+PHBV/PCL group). This might be related to the very high bioactivity of the scaffolds that might induce osteogenic activities at an early time point (Jodati et al., 2022). Among groups, 5% BAG had the highest cell viability on days 4 and 7. The viability changes were very small between groups and contradictory with Ba content for different BAG % groups.

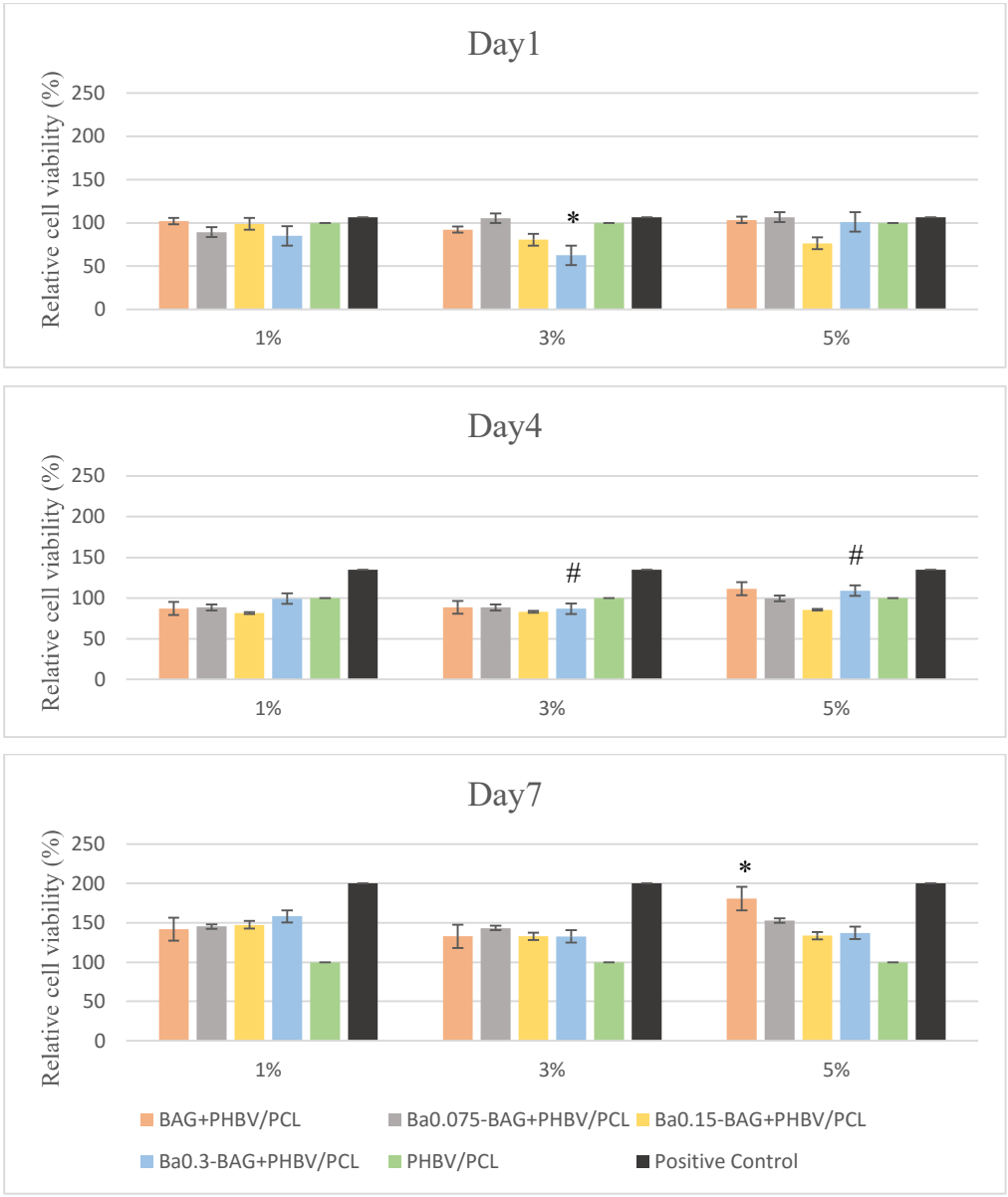

Figure 4.10. Relative viability of Saos-2 cells on pure and Ba-doped BAG incubated for 1, 4, and 7 days. The error bars represent the standard error of means. * indicates a statistically significant difference (<0.05) between scaffold groups and PHBV/PCL. A statistically significant difference (<0.05) between the same groups with increasing Ba-doped BAG amount indicated with #. Viability on pure PHBV/PCL was accepted as 100%.

As mentioned before, both nano and microfibers were observed in the structure, thus scaffolds in this study are expected to promote better cell attachment as well as cell

growth. In the study on BAG (Jodati et al., 2022) it has been reported that BAG has no cytotoxic effects on Saos-2 cells, and it can enhance cell attachment and viability. This non-toxic effect of BAG was reported in another study on Zn-doped BAG (Yadav et al., 2021). The same results in this thesis confirmed the non-toxic effect of BAG-containing scaffolds on direct contact with Saos-2 cells after 7 days of incubation. Finally, in a study on Ba-doped Bioglass (Arepalli et al., 2015) it has been reported that in low concentrations barium can promote cell proliferation. In another study on HA-Ba (Tavangar et al., 2020) it has been reported that the cellular proliferation of pure barium titanate is significantly lower than the ones doped with HA, which indicates the toxic effects of Ba when used at high concentrations. In this thesis, doping BAG with Ba and then electrospinning with PHBV/PCL formed scaffolds with non-toxic effects on Saos-2 cells. It is also suggestible that low Ba doping amounts might also have a controllable effect on cell viability. Saos-2 cells have a doubling time of 48 h, so day 1 results can be considered to be mostly reflecting initially attached cells' viability. However, on day 4 we expect proliferation and this was very low in all groups.

After analyzing the cell viability of scaffolds after days 1 and 7, scaffolds were fixed for SEM analysis, in order to control the cells. The SEM analysis of scaffolds is presented in Figure 4.11. The presence of cells was observed on the surface of scaffolds after day1, but on day 7 very low amount of cells (even no cells in some of the scaffolds) were observed on the surface, which indicated that after 7 days of incubation, cells were moved inside the fibers. Saos-2 cells seeded on PHBV/PCL scaffolds had round morphology which indicates poor interaction with fibers. The number of cells was slightly increased with the BAG amount. These findings are in agreement with the literature (Dalgic et al., 2019).

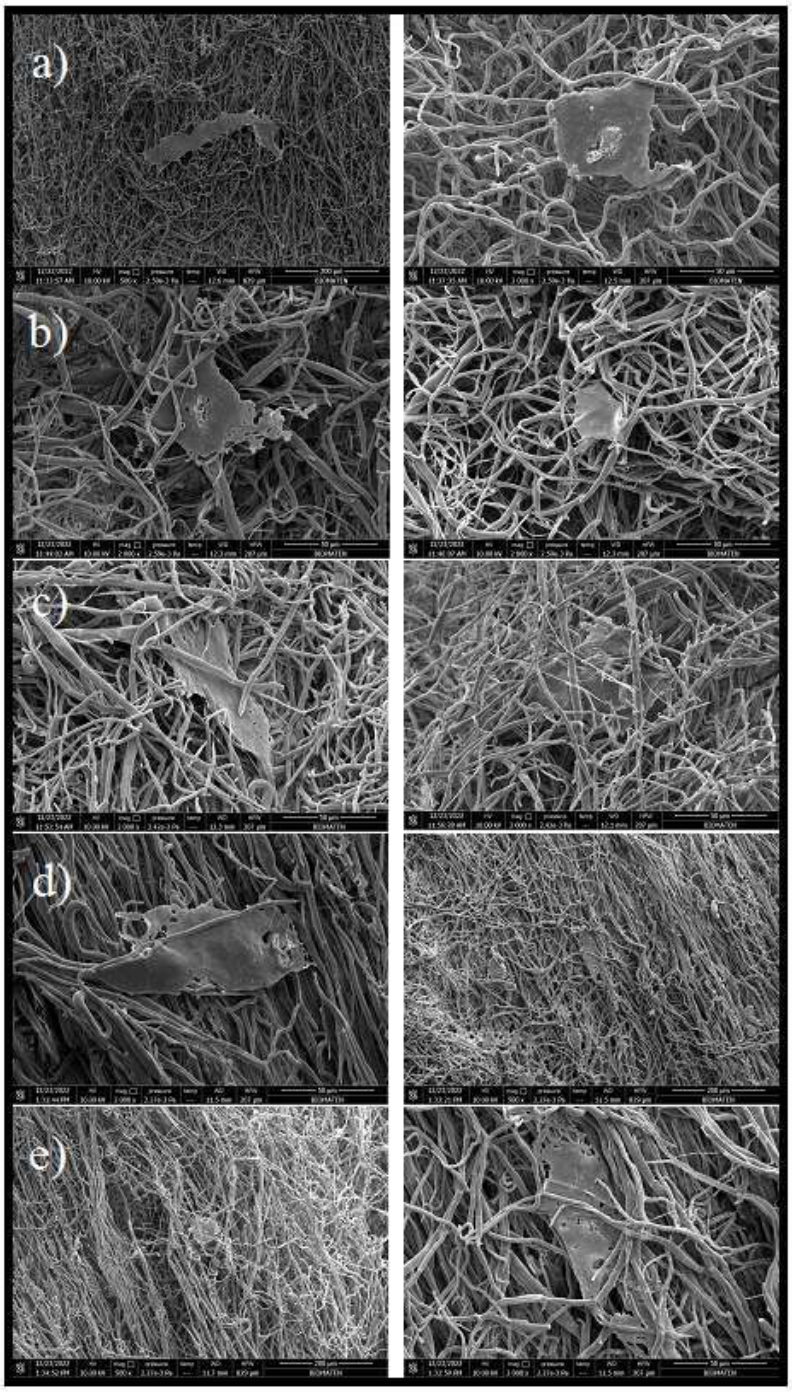

Figure 4.11. SEM image of scaffolds after day 1. a) BAG5%+PHBV/PCL, b)$Ba_{0.075}$-BAG5%+PHBV/PCL, c) $Ba_{0.15}$-BAG+PHBV/PCL, d) $Ba_{0.3}$-BAG+PHBV/PCL, e) PHBV/PCL

4.2.2.2 Alkaline Phosphate (ALP) Activity Test Results

ALP is produced by osteoblast cells during active bone resorption, making it one of the earliest indicators of osteogenic differentiation (Watts, 1999). To investigate the effect of Ba ions in the structure of BAG+PHBV/PCL scaffolds, on the osteogenic activity of Saos-2 cells, ALP activity was determined. ALP activity of Saos-2 cells on BAG and Ba-doped BAG incorporated with PHBV/PCL scaffolds after 7 and 14 days of incubation are presented in Figure 4.12.

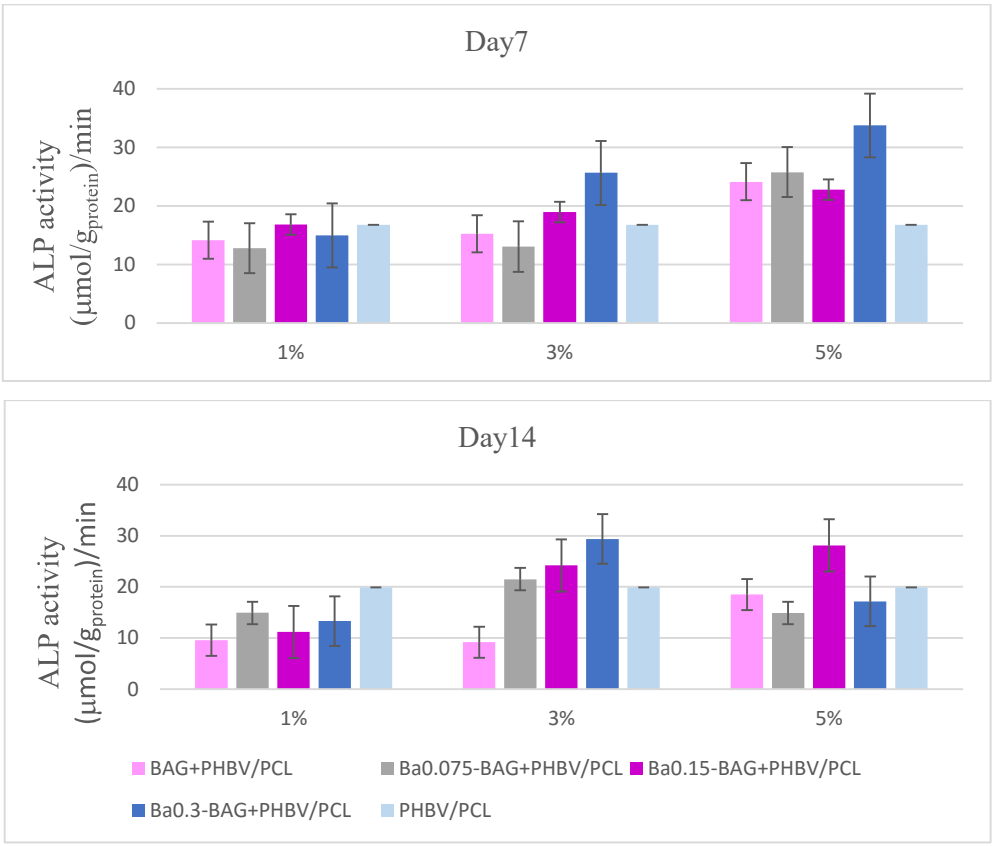

Figure 4.12. ALP activity of Saos-2 cells seeded on scaffold groups and incubated in the osteogenic medium at 37°C for 7 and 14 days (n=3). The error bars represent the standard error of means.

Among samples, the ALP activity of cells on 1% BAG+PHBV/PCL and Ba-doped BAG +PHBV/PCL barely had an effect on the samples. At day 7, all the samples of 5% BAG and Ba-doped BAG had higher ALP activity than observed in PHBV/PCL

(control group). At day 7, 2-fold higher ALP activity was observed for $Ba_{0.3}$-BAG5%+PHBV/PCL and 1.3-1.5-fold higher ALP activity was observed for $Ba_{0.075}$-BAG5%+PHBV/PCL, and $Ba_{0.15}$-BAG5%+PHBV/PCL groups compared with the control group. These results are also in agreement with cell viability results (Figure 4.10). At day 7, $Ba_{0.15}$-BAG3% +PHBV/PCL and $Ba_{0.3}$-BAG3%+PHBV/PCL groups showed higher ALP activity than the control group too.

$Ba_{0.3}$-BAG5%+PHBV/PCL had reached its highest value at day 7 and decrease at day 14. BAG5%+PHBV/PCL and $Ba_{0.075}$-BAG5%+PHBV/PCL showed the same behavior, but $Ba_{0.15}$-BAG5%+PHBV/PCL kept rising. Among samples, Ba-doped BAG5%+PHBV/PCL gave the highest ALP activity results. No statistically significant difference was observed among groups compared with PHBV/PCL.

It had been reported in a study (Jodati et al., 2022), that BAG can promote the osteogenic activity of cells. This result suggested that BAG's osteogenic property may help explain why it is a strong candidate for treating bone defects. In another study (Tavangar et al., 2020) it had been reported that there is no significant difference between the ALP activity of pure HA and Ba-doped HA.

The amount of intracellular calcium after 7 and 14 days of incubation in the osteogenic medium is presented in Figure 4.13. As shown all of the scaffold groups have higher intracellular calcium than PHBV/PCL.

In parallel with ALP activity results (and by considering the statistical analysis), the highest intracellular calcium accumulation was observed in scaffolds containing $Ba_{0.15}$-BAG and $Ba_{0.3}$-BAG. Although $Ba_{0.15}$-BAG and $Ba_{0.3}$-BAG containing groups differed from the control groups, there was no significant difference among themselves. Similar to the ALP activity of scaffold groups, 1% BAG and Ba-doped BAG groups had no significant effect.

The intracellular Ca accumulation of scaffold groups was decreased on day 14. These results were parallel to ALP activity results.

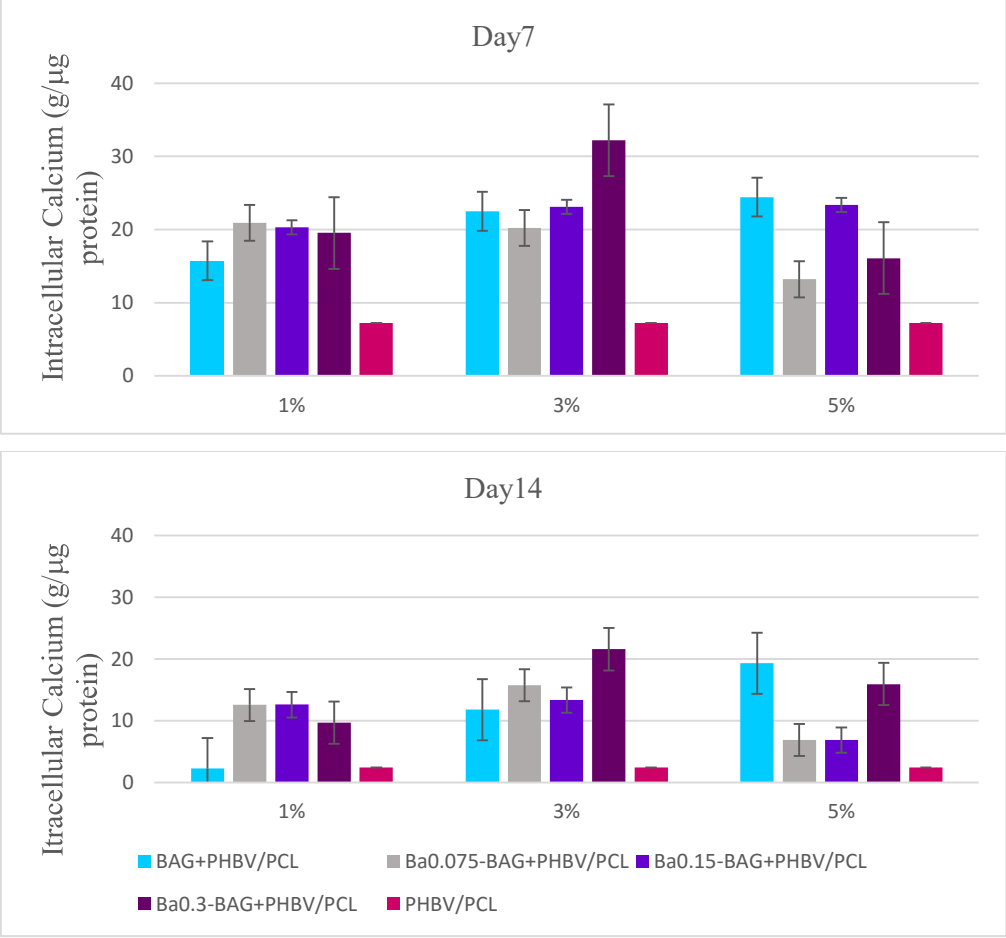

Figure 4.13. The amount of intracellular calcium accumulation of Saos-2 cells seeded on composite scaffolds. The error bars represent the standard error of means (n=3).

4.2.3 Mechanical Properties

As (Kariem et al., 2015) studied the relationship between the porosity and stiffness of BAG scaffolds fabricated using the polymer sponge replica method, they estimated the mechanical properties of BAG as a potential biomaterial. The results confirmed the inverse relation between porosity and stiffness of polycrystalline ceramics. The different methods were used to fabricate porous BAG scaffolds with

interconnected pores, and the results were compared with the mechanical properties of human compact and trabecular bones and HA scaffolds. Results of these studies indicated that BAG scaffolds with porosity of 75% and pore size of 200-500 μm had a suitable compressive strength, which makes BAG scaffolds an appropriate candidate for spongy bone tissue regeneration (Gerhardt and Boccaccini, 2010; Kunjalukkal Padmanabhan et al., 2013; Sadeghzade et al., 2017). In a study on PHBV/PCL scaffolds that were prepared using the electrospinning method (Dalgic et al., 2019), it has been indicated that PHBV/PCL scaffolds had low compressive strength, but the compressive strength of scaffolds was enhanced using diatoms (DS). Incorporating DS into PHBV/PCL scaffolds resulted in increased fiber size, on the other hand, DS particles fill some of the pores which resulted in a very small improvement in physical support within fiber mesh, thus, the higher compressive strength. But it has been stated that the main reason for the improved compressive strength of PHBV/PCL/DS is lower porosity and higher fiber density than PHBV/PCL scaffolds. It has been reported that the compressive strength of apatite is exponentially dependent on porosity (RAO WR et al., 1974). In a study on BAG scaffolds prepared by sol-gel methods (Jodati et al., 2022), it has been reported that different porosity can be addressed as the main reason for observing different compressive strengths.

Doping Ba into HA resulted in a decrease in the porosity of scaffolds (Tavangar et al., 2020), and this decrease in the porosity increased the compressive strength of scaffolds containing Ba in their structure. In the mentioned study, the decrease in the porosity and the increase in the mechanical properties of scaffolds were attributed to the size of initial particles of HA and Ba.

In this thesis, a compression test was performed in 6 groups of samples. After getting the results of cell viability tests on scaffolds, the group containing 5% BAG and Ba-doped BAG was chosen for compression test to evaluate the effect of increasing Ba on scaffolds. In addition to this group, 3% BAG and PHBV/PCL were included to

check the effect of increasing BAG on the scaffolds. The results are presented in Table 4.8.

Table 4.8 Compressive strength test results of scaffold groups (n = 3)

Scaffolds Groups	Compressive Strength (65% strain) (kPa)	Elastic Modulus (kPa)
BAG3%+PHBV/PCL	6.92±1.23	10.58±1.87
BAG5%+PHBV/PCL	7.75±0.39	11.85±0.59
$Ba_{0.075}$-BAG5%+ PHBV/PCL	9.36±0.85	14.32±1.29#
$Ba_{0.15}$-BAG5%+ PHBV/PCL	12.02±1.49*	18.39±2.28#
$Ba_{0.3}$-BAG5%+PHBV/PCL	11.22±1.31*	17.17±2.00#
PHBV/PCL	4.25±0.70	6.51±1.16

*: Statistically significant difference in compressive strength of PHBV/PCL scaffolds containing Ba-doped BAG with PHBV/PCL scaffolds. #: Statistically significant difference of elastic modulus of PHBV/PCL scaffolds containing Ba-doped BAG with PHBV/PCL scaffolds.

Based on the results of compression tests, increasing BAG in the structure of scaffolds enhanced the compressive strength of the scaffolds. Doping Ba into BAG resulted in a decrease in the porosity of scaffolds (Table 4.7), which results in an increase in the compressive strength of scaffolds. As the Ba amount increases, so does the compressive strength. As mentioned, Ba has a greater initial size than Ca, which has been replaced by Ba in the BAG structure in the doping process, so Ba-doped BAG particles can create bigger grains compared with BAG. These bigger grains formed scaffolds with lower porosity, thus, enhance in the compressive strength and elastic modulus will be achieved.

CHAPTER 5

Conclusion

In this study BAG and Ba-doped BAG with different amounts were produced with a sol-gel method for BTE applications. The effect of the amount of Ba-doped BAG on the structural and biological properties was investigated. The structural analysis determined by XRD and FTIR on BAG and Ba-doped BAG proved that Ba can be successfully doped to the structure of BAG. When the Ba amount increased, the presence of the additional phases was reduced. The crystallinity and grain size of the samples gradually increased with increasing Ba amount. ICP-MS analysis, which determines the chemical composition of BAG and Ba-doped samples, revealed the successful doping of Ba into the BAG structure. Doping Ba into BAG structure in low concentrations did not show cytotoxic effects on Saos-2 cells. The results obtained in this study revealed that with doping Ba^{2+} ions, mechanical and biological properties of scaffolds were clearly upgraded, and samples were suggested to have potential as a biomaterial for bone implant applications.

PHBV/PCL scaffolds incorporating the different amounts of BAG and Ba-doped BAG were fabricated by electrospinning methods for bone regeneration applications. The effect of varying amount of BAG and Ba-doped BAG on PHBV/PCL scaffolds were examined. The porosity of the samples was reduced by increasing BAG and Ba-doped BAG amount resulting in an enhanced compressive strength. The results of this study revealed that doping Ba can control the high degradation rate of BAG. Additionally, a bioactivity study revealed that scaffolds containing Ba showed faster CaP precipitation compared to the control group and apatite accumulation in these groups was higher. The presence of pure or Ba-doped BAG was shown to improve the water uptake ability of scaffolds. Electrospinning BAG and Ba-doped BAG with PHBV/PCL polymers resulted in the formation of both micro and nanofibers which enhanced the ability of cell proliferation and osteogenic activity on samples. In the

relative cell viability (%) test, the highest viability was observed on the scaffolds with BAG. The viability changes were very small between groups and contradictory with Ba content for different BAG % groups. It was concluded that PHBV/PCL electrospun scaffold with 5% Ba-BAG has the potential to be used in BTE.

REFERENCES

Abbasian, V., Emadi, R., Kharaziha, M., 2020. Biomimetic nylon 6-baghdadite nanocomposite scaffold for bone tissue engineering. Mater. Sci. Eng. C 109, 110549. https://doi.org/10.1016/j.msec.2019.110549

Al-Hermezi, H.M., McKie, D., Hall, A.J., 1986. Baghdadite, a new calcium zirconium silicate mineral from Iraq. Mineral. Mag. 50, 119–123. https://doi.org/10.1180/minmag.1986.050.355.15

Alipal, J., Mohd Pu'ad, N.A.S., Lee, T.C., Nayan, N.H.M., Sahari, N., Basri, H., Idris, M.I., Abdullah, H.Z., 2019. A review of gelatin: Properties, sources, process, applications, and commercialisation. Mater. Today Proc. 42, 240–250. https://doi.org/10.1016/j.matpr.2020.12.922

Anatoly N. Boyandina, Sukovatiya, E.D.N. and A.G., 2016. Properties and biocompatibility of poly-3-hydroxybutyrate-co-3-hydroxyvalerate/ Poly-3-caprolactone blends. Sib. Fed. Univ. Biol. 9, 63–74. https://doi.org/10.17516/1997-1389-2015-9-1-63-74

Arefpour, A., Kasiri-Asgarani, M., Monshi, A., Doostmohammadi, A., Karbasi, S., 2019. Fabrication, characterization and examination of in vitro of baghdadite nanoparticles for biomedical applications. Mater. Res. Express 6, 14. https://doi.org/10.1088/2053-1591/ab318c

Arefpour, A., Kasiri-Asgarani, M., Monshi, A., Karbasi, S., Doostmohammadi, A., 2020. Baghdadite/polycaprolactone nanocomposite scaffolds: preparation, characterisation, and in vitro biological responses of human osteoblast-like cells (Saos-2 cell line). Mater. Technol. 35, 421–432. https://doi.org/10.1080/10667857.2019.1692161

Arepalli, S.K., Tripathi, H., Vyas, V.K., Jain, S., Suman, S.K., Pyare, R., Singh, S.P., 2015. Influence of barium substitution on bioactivity, thermal and physico-mechanical properties of bioactive glass. Mater. Sci. Eng. C 49, 549–559. https://doi.org/10.1016/j.msec.2015.01.049

Bakhsheshi-Rad, H.R., Hamzah, E., Ismail, A.F., Aziz, M., Hadisi, Z., Kashefian, M., Najafinezhad, A., 2017. Novel nanostructured baghdadite-vancomycin scaffolds: in-vitro drug release, antibacterial activity and biocompatibility. Mater. Lett. 209, 369–372. https://doi.org/10.1016/j.matlet.2017.08.027

Biagioni, C., Bonaccorsi, E., Perchiazzi, N., Merlino, S., 2010. Single crystal refinement of the structure of baghdadite from Fuka (Okayama Prefecture, Japan). Period. di Mineral. 79, 1–9. https://doi.org/10.2451/2010PM0013

Boccaccio, A., 2021. Design of materials for bone tissue scaffolds. Materials (Basel). 14, 10–13. https://doi.org/10.3390/ma14205985

Bohner, M., Lemaitre, J., 2009. Can bioactivity be tested in vitro with SBF solution? Biomaterials 30, 2175–2179. https://doi.org/10.1016/j.biomaterials.2009.01.008

Dalgic, A.D., Atila, D., Karatas, A., Tezcaner, A., Keskin, D., 2019. Diatom shell incorporated PHBV/PCL-pullulan co-electrospun scaffold for bone tissue engineering. Mater. Sci. Eng. C 100, 735–746. https://doi.org/10.1016/j.msec.2019.03.046

Daskalakis,. 2021. Bioglasses for bone tissue engineering. In: Bártolo, P.J., Bidanda, B. (eds) Bio-materials and prototyping applications in Medicine. Springer, Cham. https://doi.org/10.1007/978-3-030-35876-1_9

Donnaloja, F., Jacchetti, E., Soncini, M., Raimondi, M.T., 2020. Natural and synthetic polymers for bone scaffolds optimization. Polymers (Basel). 12, 1–27. https://doi.org/10.3390/POLYM12040905

Evis, Z., 2007. Reactions in hydroxylapatite-zirconia composites. Ceram. Int. 33, 987–991. https://doi.org/10.1016/j.ceramint.2006.02.012

Fernandez-Yague, M.A., Abbah, S.A., McNamara, L., Zeugolis, D.I., Pandit, A., Biggs, M.J., 2015. Biomimetic approaches in bone tissue engineering: Integrating biological and physicomechanical strategies. Adv. Drug Deliv. Rev. 84, 1–29. https://doi.org/10.1016/j.addr.2014.09.005

Gerhardt, L.C., Boccaccini, A.R., 2010. Bioactive glass and glass-ceramic scaffolds for bone tissue engineering. Materials (Basel). 3, 3867–3910. https://doi.org/10.3390/ma3073867

Gholamzadeh, L., Sharghi, H., Aminian, M.K., 2022. Synthesis of barium-doped PVC/Bi2WO6 composites for X-ray radiation shielding. Nucl. Eng. Technol. 54, 318–325. https://doi.org/10.1016/j.net.2021.07.045

Gregor, A., Filová, E., Novák, M., Kronek, J., Chlup, H., Buzgo, M., Blahnová, V., Lukášová, V., Bartoš, M., Nečas, A., Hošek, J., 2017. Designing of PLA scaffolds for bone tissue replacement fabricated by ordinary commercial 3D printer. J. Biol. Eng. 11, 1–21. https://doi.org/10.1186/s13036-017-0074-3

Guo, L., Liang, Z., Yang, L., Du, W., Yu, T., Tang, H., Li, C., Qiu, H., 2021. The role of natural polymers in bone tissue engineering. J. Control. Release 338, 571–582. https://doi.org/10.1016/j.jconrel.2021.08.055

Ibrahim, M.I., Alsafadi, D., Alamry, K.A., Hussein, M.A., 2021. Properties and applications of poly(3-hydroxybutyrate-co-3-hydroxyvalerate) biocomposites. J. Polym. Environ. 29, 1010–1030. https://doi.org/10.1007/s10924-020-01946-x

Jodati, H., Tezcaner, A., Evis, Z., Alshemary, A.Z., Çelik, E., 2022. Synthesis of baghdadite using modified sol–gel route and investigation of its properties for bone treatment applications. J. Korean Ceram. Soc. inprint.

https://doi.org/10.1007/s43207-022-00275-0

Jodati, H., Yilmaz, B., Evis, Z., 2020. Calcium zirconium silicate (baghdadite) ceramic as a biomaterial. Ceram. Int. 46, 21902–21909. https://doi.org/10.1016/j.ceramint.2020.06.105

Jokanović, V., Čolović, B., Popović-Bajić, M., Živković-Sandić, M., 2019. Scaffold in bone tissue engineering. Stomatol. Glas. Srb. 64, 32–40. https://doi.org/10.1515/sdj-2017-0004

Jones, J.R., 2015. Reprint of: Review of bioactive glass: From Hench to hybrids. Acta Biomater. 23, S53–S82. https://doi.org/10.1016/j.actbio.2015.07.019

Kariem, H., Pastrama, M.I., Roohani-Esfahani, S.I., Pivonka, P., Zreiqat, H., Hellmich, C., 2015. Micro-poro-elasticity of baghdadite-based bone tissue engineering scaffolds: A unifying approach based on ultrasonics, nanoindentation, and homogenization theory. Mater. Sci. Eng. C 46, 553–564. https://doi.org/10.1016/j.msec.2014.10.072

Kokubo, T., Takadama, H., 2006. How useful is SBF in predicting in vivo bone bioactivity? Biomaterials 27, 2907–2915. https://doi.org/10.1016/j.biomaterials.2006.01.017

Kosmač, T., Kocjan, A., 2012. Ageing of dental zirconia ceramics. J. Eur. Ceram. Soc. 32, 2613–2622. https://doi.org/10.1016/j.jeurceramsoc.2012.02.024

Kunjalukkal Padmanabhan, S., Gervaso, F., Carrozzo, M., Scalera, F., Sannino, A., Licciulli, A., 2013. Wollastonite/hydroxyapatite scaffolds with improved mechanical, bioactive and biodegradable properties for bone tissue engineering. Ceram. Int. 39, 619–627. https://doi.org/10.1016/j.ceramint.2012.06.073

Lacerda, C.M.R., 2018. Biomaterials for bone tissue engineering. Bone Regen. Concepts, Clin. Asp. Futur. Dir. 231–254. https://doi.org/10.1002/9783527603978.mst0481

Li, J.J., Roohani-Esfahani, S.I., Dunstan, C.R., Quach, T., Steck, R., Saifzadeh, S., Pivonka, P., Zreiqat, H., 2016. Efficacy of novel synthetic bone substitutes in the reconstruction of large segmental bone defects in sheep tibiae. Biomed. Mater. 11, 15016. https://doi.org/10.1088/1748-6041/11/1/015016

Li, Y., Liu, Y., Li, R., Bai, H., Zhu, Z., Zhu, L., Zhu, C., Che, Z., Liu, H., Wang, J., Huang, L., 2021. Collagen-based biomaterials for bone tissue engineering. Mater. Des. 210. 0264-1275. https://doi.org/10.1016/j.matdes.2021.110049

Lü, L.X., Wang, Y.Y., Mao, X., Xiao, Z.D., Huang, N.P., 2012. The effects of PHBV electrospun fibers with different diameters and orientations on growth behavior of bone-marrow-derived mesenchymal stem cells. Biomed. Mater. 7 015002. 1748-6041. https://doi.org/10.1088/1748-6041/7/1/015002

Maia, F.R., Bastos, A.R., Oliveira, J.M., Correlo, V.M., Reis, R.L., 2022. Recent approaches towards bone tissue engineering. Bone 154. 8756-3282

https://doi.org/10.1016/j.bone.2021.116256

Martel, A., Olivas-armendariz, I., 2016. Biocomposites scaffolds for bone tissue engineering. Int. J. Compos. Mater. 5, 167–176. https://doi.org/10.5923/j.cmaterials.20150506.05

Mugundan, S., Praveen, P., Sridhar, S., Prabu, S., Lawrence Mary, K., Ubaidullah, M., Shaikh, S.F., Kanagesan, S., 2022. Sol-gel synthesized barium doped TiO2 nanoparticles for solar photocatalytic application. Inorg. Chem. Commun. 139, 109340. https://doi.org/10.1016/j.inoche.2022.109340

Perić Kačarević, Ž., Rider, P., Alkildani, S., Retnasingh, S., Pejakić, M., Schnettler, R., Gosau, M., Smeets, R., Jung, O., Barbeck, M., 2020. An introduction to bone tissue engineering. Int. J. Artif. Organs 43, 69–86. https://doi.org/10.1177/0391398819876286

Piconi, C., Maccauro, G., 1999. Zirconia as a ceramic biomaterial. Biomaterials 20, 1–25. https://doi.org/10.1016/S0142-9612(98)00010-6

Poitout, D.G., 2016. Biomechanics and biomaterials in orthopedics, second edition. Biomech. Biomater. Orthop. Second Ed. 1–547. https://doi.org/10.1007/978-1-84882-664-9

Popescu, R.C., Souto, E.M.B., 2019. Innovative biomaterials in bone tissue Engineering. Mater. Int. 1, 33263.

Rao WR, Boehm RF., 2009 A study of sintered apatites. Journal of Dental Research. 1974;53(6):1351-1354. https://doi.org/10.1177/00220345740530061001

Roohani-Esfahani, S.I., Dunstan, C.R., Davies, B., Pearce, S., Williams, R., Zreiqat, H., 2012. Repairing a critical-sized bone defect with highly porous modified and unmodified baghdadite scaffolds. Acta Biomater. 8, 4162–4172. https://doi.org/10.1016/j.actbio.2012.07.036

Sachlos, E., Czernuszka, J.T., Gogolewski, S., Dalby, M., 2003. Making tissue engineering scaffolds work. Review on the application of solid free form fabrication technology to the production of tissue engineering scaffolds. Eur. Cells Mater. 5, 29–40. https://doi.org/10.22203/ecm.v005a03

Sadeghpour, S., Amirjani, A., Hafezi, M., Zamanian, A., 2014. Fabrication of a novel nanostructured calcium zirconium silicate scaffolds prepared by a freeze-casting method for bone tissue engineering. Ceram. Int. 40, 16107–16114. https://doi.org/10.1016/j.ceramint.2014.07.039

Sadeghzade, S., Emadi, R., Ahmadi, T., Tavangarian, F., 2019. Synthesis, characterization and strengthening mechanism of modified and unmodified porous diopside/baghdadite scaffolds. Mater. Chem. Phys. 228, 89–97.

https://doi.org/10.1016/j.matchemphys.2019.02.041

Sadeghzade, S., Emadi, R., Tavangarian, F., Doostmohammadi, A., 2020. In vitro evaluation of diopside/baghdadite bioceramic scaffolds modified by polycaprolactone fumarate polymer coating. Mater. Sci. Eng. C 106, 110176. https://doi.org/10.1016/j.msec.2019.110176

Sadeghzade, S., Shamoradi, F., Emadi, R., Tavangarian, F., 2017. Fabrication and characterization of baghdadite nanostructured scaffolds by space holder method. J. Mech. Behav. Biomed. Mater. 68, 1–7. https://doi.org/10.1016/j.jmbbm.2017.01.034

Samani, D.A., Doostmohammadi, A., Nilforoushan, M.R., Nazari, H., 2019. Electrospun polycaprolactone/graphene/baghdadite composite nanofibres with improved mechanical and biological properties. Fibers Polym. 20, 982–990. https://doi.org/10.1007/s12221-019-1161-5

Schumacher, T.C., Volkmann, E., Yilmaz, R., Wolf, A., Treccani, L., Rezwan, K., 2014. Mechanical evaluation of calcium-zirconium-silicate (baghdadite) obtained by a direct solid-state synthesis route. J. Mech. Behav. Biomed. Mater. 34, 294–301. https://doi.org/10.1016/j.jmbbm.2014.02.021

Sehgal, R.R., Roohani-Esfahani, S.I., Zreiqat, H., Banerjee, R., 2017. Nanostructured gellan and xanthan hydrogel depot integrated within a baghdadite scaffold augments bone regeneration. J. Tissue Eng. Regen. Med. 11, 1195–1211. https://doi.org/10.1002/term.2023

Senthilkumar, G., Kaliaraj, G.S., Vignesh, P., Vishwak, R.S., Joy, T.N., Hemanandh, J., 2021. Hydroxyapatite - barium/strontium titanate composite coatings for better mechanical, corrosion and biological performance. Mater. Today Proc. 44, 3618–3621. https://doi.org/10.1016/j.matpr.2020.09.758

Siriphannon, P., Kameshima, Y., Yasumori, A., Okada, K., Hayashi, S., 2002. Formation of hydroxyapatite on CaSiO3 powders in simulated body fluid. J. Eur. Ceram. Soc. 22, 511–520. https://doi.org/10.1016/S0955-2219(01)00301-6

Sombatmankhong, K., Sanchavanakit, N., Pavasant, P., Supaphol, P., 2007. Bone scaffolds from electrospun fiber mats of poly(3-hydroxybutyrate), poly(3-hydroxybutyrate-co-3-hydroxyvalerate) and their blend. Polymer. 48, 1419–1427. https://doi.org/10.1016/j.polymer.2007.01.014

Stevens, M.M., 2008. Biomaterials for bone tissue engineering. Bone 11, 18–25. https://doi.org/10.1016/S1369-7021(08)70086-5

Tavangar, M., Heidari, F., Hayati, R., Tabatabaei, F., Vashaee, D., Tayebi, L., 2020. Manufacturing and characterization of mechanical, biological and dielectric properties of hydroxyapatite-barium titanate nanocomposite scaffolds. Ceram. Int. 46, 9086–9095. https://doi.org/10.1016/j.ceramint.2019.12.157

G.C. Wang, Z.F. Lu, H. Zreiqat, 2014, Bioceramics for skeletal bone regeneration, Editor(s): Kajal Mallick, In Woodhead Publishing Series in Biomaterials, Bone Substitute Biomaterials, Pages 180-216, ISBN 9780857094971, https://doi.org/10.1533/9780857099037.2.180.

Watts, N.B., 1999. Clinical utility of biochemical markers of bone remodeling. Clin. Chem. 45, 1359–1368. https://doi.org/10.1093/clinchem/45.8.1359

Wu, C., Chang, J., 2013. A review of bioactive silicate ceramics. Biomed. Mater. 8, 032001. https://doi.org/10.1088/1748-6041/8/3/032001

Wu, T., Yu, S., Chen, D., Wang, Y., 2017. Bionic design, materials and performance of bone tissue scaffolds. Materials (Basel). 10, 1187. https://doi.org/10.3390/ma10101187

Wu, X., Walsh, K., Hoff, B.L., Camci-Unal, G., 2020. Mineralization of biomaterials for bone tissue engineering. Bioengineering 7, 1–24. https://doi.org/10.3390/bioengineering7040132

Xue, X., Hu, Y., Wang, S., Chen, X., Jiang, Y., Su, J., 2022. Fabrication of physical and chemical crosslinked hydrogels for bone tissue engineering. Bioact. Mater. 12, 327–339. https://doi.org/10.1016/j.bioactmat.2021.10.029

Yadav, S., Shreyasi majumdar, Ali, A., Krishnamurthy, S., Singh, P., Pyare, R., 2021. In-vitro analysis of bioactivity, hemolysis, and mechanical properties of Zn substituted calcium zirconium silicate (baghdadite). Ceram. Int. 47, 16037–16053. https://doi.org/10.1016/j.ceramint.2021.02.178

Yedekçi, B., Tezcaner, A., Yılmaz, B., Demir, T., Evis, Z., 2022. 3D porous PCL-PEG-PCL / strontium, magnesium and boron multi-doped hydroxyapatite composite scaffolds for bone tissue engineering. J. Mech. Behav. Biomed. Mater. 125. 1751-6161. https://doi.org/10.1016/j.jmbbm.2021.104941

Zafar, M.J., Zhu, D., Zhang, Z., 2019. 3D printing of bioceramics for bone tissue engineering. Materials (Basel). 12 (20), 3361 https://doi.org/10.3390/ma12203361